Personal File

Permanent File Copy
St. Anthony Falls Hydraulic Laborat

UNIVERSITY OF MINNESOTA
ST. ANTHONY FALLS HYDRAULIC LABORATORY
LORENZ G. STRAUB, Director

Technical Paper No. 26, Series B

Two-Phase Flow Studies in Horizontal Pipes with Special Reference to Bubbly Mixtures

by

WALTER JAMES and EDWARD SILBERMAN

September 1958
Minneapolis, Minnesota

UNIVERSITY OF MINNESOTA
ST. ANTHONY FALLS HYDRAULIC LABORATORY
LORENZ G. STRAUB, Director

Technical Paper No. 26, Series B

Two-Phase Flow Studies in Horizontal Pipes with Special Reference to Bubbly Mixtures

by

WALTER JAMES and EDWARD SILBERMAN

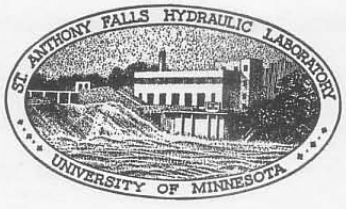

September 1958
Minneapolis, Minnesota

Reproduction in whole or in part is permitted
for any purpose of the United States Government

PREFACE

The studies described in this paper were sponsored by the David Taylor Model Basin under Contract Nonr 710(21). The contract was effective January 1, 1957, and was scheduled to terminate September 30, 1958. The contract has actually been extended, but this report covers the work through the original completion date. The contract called for "a literature search and experimental and analytic studies on the mechanics and limitations of conveying air-water mixtures through closed conduits," and can be looked upon as a resumption of an earlier contract, Nonr 710(07), which terminated in December 1954.

The entire program was under the general direction of Dr. Lorenz G. Straub, Director of the St. Anthony Falls Hydraulic Laboratory. The experimental work and data reduction were performed at various times by Tuncay Aydinalp, Athanasios Patitsas, Darrell E. Anderson, Robert L. Steele, and Hsing Chuang. Special thanks is given to Mr. Chuang who was associated with the project longer than any of the others.

The manuscript was prepared for printing by Delores Grupp and Mary Anne Peterson under the general supervision of Loyal Johnson. Thanks is given to these people as well as to the shop men who built the apparatus and to the draftsmen who worked on the report.

A B S T R A C T

An investigation has been made of the flow of bubbly mixtures in horizontal pipes, together with some related work on other flow patterns. Pressure drop is calculated through the use of a conventional friction factor. In the bubble-flow regime, it is found that the friction factor is approximately equal to or slightly greater than the friction factor for liquid flowing alone in the pipe. The bubbles move at nearly the mean velocity of the liquid while their size is inversely proportional to the liquid velocity and directly proportional to the square root of the pipe diameter.

The use of a friction factor for calculating pressure drop for other than bubble flow may also be useful, but more study is necessary to determine friction factors.

C O N T E N T S

LIST OF ILLUSTRATIONS

LIST OF TABLES

LIST OF SYMBOLS

A - Area of flow.

a,b - Constants.

D - Pipe diameter.

d - Bubble diameter, measured at atmospheric conditions.

d' - Dimensionless bubble diameter, $d' = V_\ell d\sqrt{\rho/\sigma D}$.

f - Friction factor.

G - Weight per unit time.

g - Gravitational constant.

P - Pressure.

$P_L = w_L RT$.

Q - Volume per unit time.

R - Gas constant.

R_L - Liquid fraction, A_L/A; R_G - gas fraction, A_G/A.

Re - Reynolds number, $Re = VD\rho/\mu$.

r - Pipe radius.

T - Temperature.

V - Mean velocity.

$V_\ell = Q_L/A$.

$V_* = \sqrt{\tau_o/\rho}$.

w - Specific weight.

x - Variable distance along pipe.

y - Distance from wall.

$\alpha = G_G/G_L$, mass flow ratio.

Δ - Increment.

θ - Compressibility parameter, $[\alpha/(1 + \alpha)]\ (gRT/V_\ell^2)$.

$\lambda = \sqrt{\frac{w_G}{0.075}} \times \frac{w_L}{62.3}$, Baker's parameter [2] (w in pounds per cubic foot).

μ - Viscosity.

$\pi(x)$ - Pressure parameter, $Q_L/Q_G(x) = P(x)/\alpha P_L$.

$\rho = w/g$, Density.

σ - Surface tension.

τ_o - Local mean wall shear stress around perimeter.

$\Psi = \frac{73.3}{\sigma} \left[\mu_L \left(\frac{62.3}{w_L} \right)^2 \right]^{1/3}$, Baker's parameter [2] (σ in dynes per centimeter, μ_L in centipoises, w_L in pounds per cubic foot).

Subscript L - Liquid.
Subscript G - Gas.
} No subscript means mixture.

Subscript m - Mean or average value.

TWO-PHASE FLOW STUDIES IN HORIZONTAL PIPES WITH SPECIAL REFERENCE TO BUBBLY MIXTURES

I. INTRODUCTION

Gas-liquid mixture flows are subject to a fairly complex series of flow patterns. For the purposes of this paper, these flow patterns may be described as follows:

(1) Bubble flow, in which separate bubbles of gas move along the pipe with approximately the same velocity as the liquid. These bubbles can be uniformly distributed in the pipe or they can move along in the upper region of a horizontal pipe with pure liquid flowing in the lower region.

(2) Plug flow, in which bubbles in the upper part of a horizontal pipe aglomerate to form large bubbles or plugs. Plug flow occurs at low ratios of gas-to-liquid flow.

(3) Slug flow, in which a more or less well-defined interface separates liquid and gas. The level of the interface rises and falls, and frothy slugs pass regularly along the pipe at a much greater velocity than the average liquid velocity.

(4) Annular flow, in which the liquid flows in a film around the pipe wall and the gas flows at high velicity through the central core. The film may contain gas bubbles.

(5) Mist flow, in which liquid droplets are entrained more or less uniformly throughout a gas flow. Spray flow and disperse flow have also been applied to the regime after annular flow breaks down.

(6) Separated flow, in which liquid flows along the bottom of the pipe and gas flows above. This type of flow occurs in a horizontal pipe at small liquid flow rates. If low gas-to-liquid flow ratios exist, the flow occurs with a

relatively smooth interface (stratified flow) and has characteristics approaching those of open-channel flow. If the ratio is higher, the interface is disturbed by waves (wavy flow).

This study is primarily concerned with bubble flow in horizontal pipes, but in order to delineate the limits of the bubble-flow regime, some consideration has also been given to the other patterns.

Most of the scientific investigation of two-phase flow has been conducted in the last twenty years. An extensive bibliography is contained in a summary by Santalo [1]*. The flow-pattern descriptions given above are in essential agreement with Santalo, who took his classification from Baker [2]. Baker prepared a chart, drawing on the experiments of many investigators, showing the relation of flow pattern to rate of flow. This chart is reproduced herein as Fig. 1(a) (using the nomenclature of the present paper). Baker observed that the lines on his chart actually represent regions of overlap of two flow patterns.

The bulk of the studies in horizontal pipes occurred at the University of California and resulted in the well-known Lockhart-Martinelli correlations [3, 4, 5, and 6] for pressure drop. Apparently these correlations have dominated much of subsequent two-phase flow studies. The Lockhart-Martinelli correlations are highly empirical, however, and are not universally applicable as has been indicated, for example, by Baker [2] and H. S. Ibsen in his discussion of a recent paper by Chisholm and Laird [6]. In the present study, improved correlating devices have been sought, especially those involving less empiricism.

There are two major parts in this report. The first, contained in Section III, following, considers gas-liquid mixture flows from the viewpoint of mean through-flow properties. In this part pressure drop and friction factor in two-phase flows are discussed.

The second part of the report, Section IV, considers details of the gas-liquid flow at a given cross section of a pipe. These details are important in applications which involve heat and mass transfer, for example. In

---

*Numbers in brackets refer to the List of References on p. 31.

the first part of Section IV, some consideration is given to the problem of determining the relation between the pattern of flow and division of the cross section between liquid and gas. In the remainder of Section IV, some experimental details associated with the bubble-flow pattern are presented. These involve bubble-size distribution and velocity-profile measurements.

II. SOME PRELIMINARY CONSIDERATIONS

The present investigation is concerned with steady mass flow of gas and liquid in a horizontal pipe of uniform cross section. The following assumptions are made throughout:

(1) No absorption or evolution of gas occurs.

(2) The gas obeys the perfect gas law.

(3) Isothermal conditions exist, the temperature of the liquid being imposed upon the gas.

(4) Vapor pressure and surface-tension effects may be ignored.

Since the weight rate of flow along the pipe G is constant, as are the liquid and gas components of weight flow, G_L and G_G, respectively,*

$$\left.\begin{aligned} G &= G_L + G_G = G_L\,(1+\alpha) \\ \text{where} \quad \alpha &= G_G/G_L \end{aligned}\right\} \qquad (1)$$

is a constant for a given flow.

The total volume rate of flow Q at any position along the pipe x is

$$\left.\begin{aligned} Q(x) &= Q_L + Q_G\,(x) = Q_L\,[1 + 1/\pi(x)] \\ \text{where} \quad \pi(x) &= Q_L/Q_G(x) \end{aligned}\right\} \qquad (2)$$

but $$Q_L/Q_G(x) = (G_L/G_G)\,[w_G(x)/w_L]$$

*Symbols are summarized in the List of Symbols in addition to being defined where they first occur.

where w is the specific weight of the fluid, and since, for an ideal gas,

$$w_G(x) = P(x)/RT$$

where P is the absolute pressure, T the absolute temperature of the liquid, and R the universal gas constant,

$$\left.\begin{aligned} \pi(x) &= Q_L/Q_G(x) = P(x)/(\alpha P_L) \\ \text{where} \qquad P_L &= w_L RT \end{aligned}\right\} \tag{3}$$

It is seen that π is a dimensionless pressure parameter (π corresponds to $1/\beta$ of Reference [7]).

The specific weight of the mixture is

$$w(x) = G/Q(x) = w_L\,(1 + \alpha)/[1 + 1/\pi(x)] \tag{4}$$

and the mixture velocity is

$$\left.\begin{aligned} V(x) &= Q(x)/A = V_\ell[1 + 1/\pi(x)] \\ \text{where} \qquad V_\ell &= Q_L/A \end{aligned}\right\} \tag{5}$$

and A is the cross-sectional area of the pipe; V_ℓ is a fictitious velocity of the liquid that would exist if there were no gas flow.

If an instantaneous cross-sectional view of the two-phase flow is taken, a part of the flow area (A_L) will be occupied by liquid and the remainder (A_G) by gas. The liquid fraction R_L and gas fraction R_G are defined as:

$$R_L(x) = A_L(x)/A,\ R_G(x) = A_G(x)/A,\ R_L + R_G = 1 \tag{6}$$

The mean velocities of the liquid and gas portions of the flow are

$$V_L(x) = Q_L/A_L(x) \quad \text{and} \quad V_G(x) = Q_G(x)/A_G(x) \tag{7}$$

Using Eqs. (6), (7), and (3),

$$R_G(x)/R_L(x) = A_G(x)/A_L(x) = \frac{Q_G(x)}{Q_L} \cdot \frac{V_L(x)}{V_G(x)} = \frac{1}{\pi(x)} \frac{V_L(x)}{V_G(x)} \tag{8}$$

In the preceding expressions (x) has been used to make clear the dependence on position along the pipe of certain of the variables. This symbolism will be dropped in most of the remainder of the paper, but the dependence on x of these variables should not be forgotten.

Two additional parameters (which are empirical) used by Baker [2] and appearing in Fig. 1 also require definition. These are:

$$\left.\begin{aligned} \lambda &= \sqrt{\frac{w_G}{0.075} \frac{w_L}{62.3}} \\ \text{and} \quad \psi &= \frac{73.3}{\sigma} \left[\mu_L \left(\frac{62.3}{w_L} \right)^2 \right]^{1/3} \end{aligned}\right\} \tag{9}$$

The w's are in pounds per cubic foot, the surface tension σ in dynes per centimeter, and the viscosity μ in centipoises in these parameters. It should be noted than when water near room temperature is used as the liquid, $\psi \approx 1$ and $\lambda = 28.8 \sqrt{\pi\alpha}$. Hence, with water near room temperature, the abscissa in Fig. 1(a) can be written in the alternative forms

$$\frac{\alpha}{\lambda \psi} \approx \frac{\alpha}{\lambda} = \frac{1}{28.8} \sqrt{\frac{\alpha}{\pi}} = \frac{\lambda}{\pi(28.8)^2} \tag{10a}$$

while the ordinate can be written

$$\frac{G_G}{A\lambda} = \frac{\alpha}{\lambda} \frac{G_L}{A} \approx \frac{\alpha}{\lambda\psi} \frac{G_L}{A} \tag{10b}$$

In Fig. 1(b), Baker's diagram has been replotted with G_L/A as ordinate using $\psi \approx 1$. It can be seen from the figure that a large part of the overlap region

between bubble flow on the one hand and slug or plug flow on the other occurs for $G_L/A \approx 500$ lb/sec-ft^2. In fact, all lines of constant G_L/A for $\psi \approx 1$ in Fig. 1(a) make 45-degree angles with the abscissa.

III. PRESSURE DROP AND FRICTION FACTOR

In a project report dealing with an earlier portion of the two-phase flow studies [7] it was found that for very small ratios of gas-to-liquid flow, the pressure drop in a bubbly mixture flowing in a pipe could be calculated approximately by treating the mixture as incompressible and using the corresponding incompressible friction factor. There is some mixture ratio, however, beyond which the mixture can no longer be treated as incompressible. Then the pressure drop will vary with the pressure in addition to its variation with pipe wall friction.

A. The Basic Equation for Pressure Drop

With application to bubble flow in mind, it is assumed that the gas-liquid mixture is homogeneous. A free-body analysis is carried out on a section of mixture of length Δx flowing in a circular horizontal pipe of constant cross-sectional area A and diameter D. Applying Newton's first law to this free body in the direction of flow produces the equation

$$AP(x) - \frac{4A}{D}\Delta x\, \tau_o\,(x + \Delta x/2) - AP\,(x + \Delta x) =$$

$$A\Delta x\,\frac{w(x + \Delta x/2)}{g}\cdot\frac{V(x + \Delta x) - V(x)}{\Delta t}$$

Here $\tau_o(x)$ is the average unit shear stress around the perimeter of the cross section at any x-position. After canceling out the common factors, rearranging the terms, replacing $\Delta x/\Delta t$ by $V(x + \Delta x/2)$, dividing by Δx, and letting $\Delta x \to 0$, this equation reduces to

$$\frac{dP(x)}{dx} + \frac{4\,\tau_o(x)}{D} + \frac{w(x)\,V(x)}{g}\,\frac{dV(x)}{dx} = 0 \qquad (11)$$

This differential equation describes the local conditions at x.

If there were only liquid flowing in the pipe, the third term in Eq. (11) would be zero and the equation would reduce to the condition for steady, uniform, incompressible flow. For incompressible flow, the pressure drip is conveniently expressed in terms of a friction factor f such that

$$\frac{dP}{dx} + \frac{f}{D}\frac{w_L V_\ell^2}{2g} = 0 \tag{12}$$

with

$$f = \frac{8g\,\tau_o}{w_L V_\ell^2} \tag{13a}$$

and where g is the acceleration of gravity. In compressible flow of a single fluid, the same friction factor defined as

$$f(x) = \frac{8g\,\tau_o(x)}{w_G(x)\,(Q_G(x)/A)^2} \tag{13b}$$

is applicable for finding the frictional wall shear stress [8, p. 414]. Now let it be assumed that for homogeneous mixture flow, the friction factor can again be used for finding the wall shear stress. In this case

$$f(x) = \frac{8g\,\tau_o(x)}{w(x)V^2(x)} \tag{13c}$$

In all of Eqs. (13), f depends on the local Reynolds number and surface roughness of the pipe only.

Upon substituting relations (5), (4), (3), and (13c) into Eq. (11), the latter can be put in the form

$$\left[\theta - \frac{\theta - 1}{\pi(x) + 1} - \frac{1}{\pi(x)}\right] d\pi(x) + \frac{f(x)\,dx}{2D} = 0 \tag{14}$$

where

$$\theta = \left(\frac{\alpha}{1 + \alpha} \right) \cdot \frac{gRT}{V_\ell^2} \tag{15}$$

This is the basic differential equation that must be integrated to determine the pressure drop along a pipe carrying a homogeneous gas-liquid mixture flow. Before integration can be performed, the variation of the friction factor $f(x)$ with x must be established.

It has already been observed that f varies only with Reynolds number and surface roughness. Reynolds number may vary along a pipe, however, being given by the following equation:

$$Re = \frac{DV\rho}{\mu} = \frac{DG}{g\mu A} = \frac{DG_L}{g\mu A}(1 + \alpha) \tag{16}$$

Here ρ is the density and μ the coefficient of viscosity of the mixture. Apparently the mixture viscosity is larger than the liquid viscosity and depends on the viscosity of the liquid and the geometric proportions of the gas-liquid mixture [9]. The geometry will change as the pressure along a pipe changes, but in this analysis it will be assumed that the change in geometry relative to the initial geometry is negligible. Since the temperature remains essentially constant at the value determined by the liquid temperature, it follows that the mixture viscosity remains essentially constant. Hence, the Reynolds number remains approximately constant under isothermal conditions, and since pipe roughness also remains constant for a given pipe, it may be assumed that the friction factor does not vary with x.

Under the above conditions Eq. (14) is readily integrated. The boundary conditions are:

$$\text{At } x = 0, \quad P(o) = P_o, \quad \pi(o) = \pi_o$$

$$\text{At } x = x_1, \quad P(x_1) = P_1, \quad \pi(x_1) = \pi_1$$

The solution is

$$\frac{fx_1}{2D} = \theta(\pi_o - \pi_1) - \ell n \left(\frac{\pi_o}{\pi_1} \right) \left(\frac{\pi_o + 1}{\pi_1 + 1} \right)^{\theta - 1} \qquad (17)$$

Since this equation consists of three dimensionless groups, any consistent set of units can be used. The friction factor group fx_1/D demands no explanation. The π group is the pressure group defined by Eq. (3); in fact, $\pi_o - \pi_1$ measures the pressure drop over the length x_1. The dimensionless number θ has not been explained before. Since the values of θ range from zero for pure liquid flow to infinity for pure gas flow, it can be regarded as a degree of compressibility parameter, i.e., a measure of how far the homogeneous mixture deviates from incompressibility (pure liquid flow). It should be noted from Eq. (15) that θ remains constant along a pipe and does not depend on local pressure.

In the development of Eq. (17), bias in favor of pure liquid flow was maintained by factoring out the properties of the liquid. If gas bias had been maintained instead, the same equation as Eq. (17) would have been obtained except for substituting $\theta = 1/\theta'$. Here θ' is zero for pure gas flow and infinite for pure liquid flow. It is shown in Appendix B that Eq. (17) reduces to the incompressible result when $G_G \longrightarrow 0$ and to the isothermal, compressible result when $G_L \longrightarrow 0$.

To obtain pressure drop from Eq. (17), it is necessary to estimate the friction factor, which is a function of Reynolds number and surface roughness. Reynolds number is given by Eq. (16); from Fig. 1, it is seen that in bubble flow, $\alpha < 10^{-2} \lambda\psi$ so that if the liquid is water and the pressure is only of the order of a few atmospheres, Eq. (9) shows that α can be neglected in Eq. (16). Hence, if it could be assumed that μ is given by its value for pure liquid, the appropriate Reynolds number would be that for the liquid component flowing alone in the pipe.

Define $$f_L = f_L \left(\frac{DG_L}{g\mu_L A}, \text{ roughness} \right)$$

Then $$f/f_L = 1.0 \qquad (18)$$

if $\mu \equiv \mu_L$ in a given pipe. This condition will be assumed to hold. Since it is known that $\mu > \mu_L$ [9], there will be a tendency to overestimate Reynolds number and, therefore, to underestimate the friction factor except for completely rough flow. Obviously, the above method for estimating f will not be correct for large α. (In fact, if α is sufficiently large, Reynolds number can be defined as

$$Re = \frac{DG_G}{g\mu A} \quad (1 + 1/\alpha)$$

so that the Reynolds number of the gas flowing alone might be more appropriate for finding f than the Reynolds number of the liquid flowing alone.)

Equation (17) is transcendental. For a given friction factor, the calculation of P_1, given P_o, can be obtained by a trial-and-error method from Eq. (17), or computer techniques can be applied. A more readily available and simpler method is desirable. Approximation formulas are useful for this purpose. Two of these are developed below by carrying out the logarithmic expansions of Eq. (17).

Since P_o, and therefore π_o, must be known in advance, Eq. (17) can be written

$$\frac{fx_1}{2D} = \theta\Delta\pi + \ell n \left(1 - \frac{\Delta\pi}{\pi_o}\right) + (\theta - 1) \ell n \left(1 - \frac{\Delta\pi}{\pi_o + 1}\right) \qquad (19)$$

where $\Delta\pi = \pi_o - \pi_1$. In using the logarithmic series expansion

$$\ell n (1 - x) = -x - \frac{x^2}{2} - \frac{x^3}{3} - \cdots, \quad -1 \leq x < 1$$

it is necessary that $\Delta\pi/\pi_o + 1) < 1$ and $\Delta\pi/\pi_o < 1$. These inequalities imply $\pi_1 + 1 > 0$ and $\pi_1 > 0$ respectively, which are true since $\pi \geq 0$, always. The rapidity of convergence depends on the smallness of these ratios. In the data analyzed later in this project,

$$\frac{\Delta\pi}{\pi_o + 1} \quad \text{and} \quad \frac{\Delta\pi}{\pi_o} \lesssim 0.5$$

and most ratios were substantially less than 0.5. The expansion is carried out to two places only, resulting in a quadratic equation in the unknown $\Delta\pi$.

$$\left[\frac{\theta\pi_o^2 + 2\pi_o + 1}{\pi_o^2(\pi_o^2 + 1)^2}\right](\Delta\pi)^2 - \frac{2(\theta\pi_o^2 - 1)}{\pi_o(\pi_o + 1)}\Delta\pi + \frac{fx_1}{D} = 0 \qquad (20)$$

This equation is solved by the quadratic formula. In order to obtain the correct incompressible formula as $G_G \to 0$, the minus sign must be taken. The result is

$$P_1 - P_o = \Delta P = P_o \Gamma \left[1 - \sqrt{1 - \frac{fx_1(\pi_o + 1)}{D\Gamma(\theta\pi_o^2 - 1)}}\right]$$

where

$$\Gamma = \frac{(\theta\pi_o^2 - 1)(\pi_o + 1)}{\theta\pi_o^2 + 2\pi_o + 1} \qquad (21)$$

If the second term under the radical is considerably less than unity, a further simplification can be made by expanding the binominal term under the radical sign. The result is:

$$\Delta P \approx \frac{P_o(\pi_o + 1)fx_1}{2D(\theta\pi_o^2 - 1)} \qquad (22)$$

For very small gas-to-liquid flow ratios, Eq. (22) becomes the incompressible equation

$$\Delta P \approx \frac{fx_1}{D}\frac{w_L}{2g}V_\ell^2$$

B. Experimental Data

Experiments were conducted for two purposes; namely, to determine the limiting conditions for bubble flow and to verify the assumptions leading to Eqs. (17) and (18) for calculating pressure drop in bubble flow. The latter experiments were conducted first and will be described first. Some additional experimental data obtained recently by Chisholm and Laird [6] and covering higher gas-liquid ratios have been used to supplement the present experiments. All of the experiments used air for the gas and water for the liquid component.

1. First Experimental Apparatus

Figure 2 is a diagrammatic sketch of the apparatus used in the initial experimental work. Actually, two pipe sizes were used in this study; 2-1/2-in. and 4-in. galvanized pipes. The 2-1/2- and 4-in. aspirators (air-water mixers) were designed and constructed for a previous project and their construction details and operating characteristics are given in the report on that project [7]. The discussion that follows will be for the 2-1/2-in. system only. The description and operation of the 4-in. system was similar except that it had no Lucite viewing sections before and after the test section.

The system was nonrecirculating. The water orifice was calibrated in place by running the discharge into a rectangular enclosure. The air nozzle was not calibrated, and the flow rate through it was computed from a theoretical formula. Some runs were made by forcing in air from the compressed-air system. In these cases the air flow was measured by a calibrated rotameter. Air was always introduced into the system through the aspirator. The test section consisted of approximately the last 17 ft of a 23-ft continuous length of pipe. Pressure-measuring connections were made at the beginning, middle, and end of this test section. Each pressure connection consisted of four symmetrically placed holes around the circumference of the pipe, all connected to a copper-tubing ring which was connected to the manometer system. Initial pressures in the test section were measured by an open manometer and a calibrated Bourdon gage. The manometer readings were used in the computations unless the initial pressure exceeded the manometer range. The pressure drops along the first half and along the whole test section were measured by a mercury U-tube manometer. The discharge valve was partially closed for some runs so that data were obtained at various levels of average system pressure. All data-taking points were preceded by sufficient lengths of pipe so that

any upstream disturbance would not affect readings taken at these points and so that turbulent flow would be fully developed.

All data necessary to compute the friction factor f as defined by Eq. (17) were taken. The data, as well as the more important computed numbers, are given in Table I (in Appendix A). When G_G equals zero, as in runs 27 and 34 of Table I, for example, $f \equiv f_L$. The range of variables covered by these data is indicated by the shading in Fig. 1. Pattern observations of the flow confirmed that all of these data were in the bubble flow regime.

The bulk of the friction-factor data from Table I has been plotted in Fig. 3, along with other data, in the form f/f_L versus Baker's abscissa, $\alpha/\lambda\psi$ for several values of G_L/A.

2. Second Experimental Apparatus

The purpose of these additional experiments was twofold. It was desired to determine the effects of a flow disturbance occurring between two straight lengths of pipe, and it was also desired to investigate the limits of the bubble-flow regime. The only disturbance employed was a 180-degree return bend. Since the average test-section pressures before and after the bend would be different because of pressure drop in the bend, the effect of system pressure on pressure drop and flow pattern would also be under study. By forcing in air from an air compressor, the upper limit of the compressibility parameter θ was increased from 2 for the previous experiments to about 200 for these experiments.

A sketch of the second system is shown in Fig. 4. It consisted basically of two identical 2-1/2-in.-pipe test sections placed before and after the return bend. Each test section consisted of the last 12 ft of a continuous 22-ft length of pipe. Air flow was measured using a calibrated orifice. The manometry system was altered halfway through the tests. Originally, each test section was provided with a mercury manometer only. Many of the readings were small enough so that it was felt that some error in the pressure-drop readings resulted. For the second half of the data, the manometry system was redesigned (details not shown) by connecting needle valves as double-pole, double-throw switches. This valving permitted the pressure drop in either test section to be measured by a Meriam No. 3 or mercury manometer. Sight glasses were installed before and after the return bend to obtain visual data on the pattern of flow.

Data were taken for a series of air flows at a constant water flow and constant initial pressure. The average system pressure of the initial test section was naturally higher than that in the final test section. As the air or water flow was changed, the pressures in both sections changed, but not in a readily comparable manner. Since it was disquieting to have the test-section pressures change in unknown manners, it was decided to hold the initial pressure of each test section at a nearly constant value for each constant water-flow series. This was done in the following manner: The first test of a constant water-flow series was conducted with maximum air flow, the back pressure valve being completely open. This test produced the highest system pressure and established the value of P_o for each test section for this series. Data from both sections were recorded. Since the air flow for the next run was less, pressures throughout the system dropped. The back pressure valve was adjusted until the value of P_o for the initial test section was restored to the same value as for the first run. Data from the initial test section were recorded. This process was repeated for the second test section. The total operation was repeated for the complete range of air settings and constant water settings. In order to obtain data from each test section under "before" and "after" conditions, and in order to insure that any unusual phenomena arising from these studies were due to a natural functioning of the system, rather than due to any errors in the system, the testing program was repeated with the test sections interchanged.

The data and computations for the second set of experimental studies are tabulated in Table II (in Appendix A). Only data taken after interchanging the test sections and improving the manometer system are shown in the table. As before, f was computed from the measured pressure drop using Eq. (17); some of these data have been plotted in Fig. 3 along with the earlier data from the first apparatus.

Flow-pattern observations were made when taking data for the initial test section (minor adjustments in the back pressure valve in regulating the initial pressure of the final test section did not seem to affect the flow pattern). The pattern observations are shown in detail in Table II and are plotted in Fig. 1. The viewing sections immediately before and after the return bend represent extreme nonsymmetry in observing the flow pattern since the pattern in the initial viewing section is reached under maximum equilibrium-establishing conditions, while the flow pattern after the bend is in a highly

disturbed condition. Even so, the pattern rarely changed significantly before and after the disturbance. The most serious effect of the bend occurred in a series (162-168) where several of the runs suffered a change from bubble flow to slight slugging flow. However, for this particular series the flow pattern changed from bubble flow for low air content to slug flow for higher air content in the upstream section. Hence, this series passed through a critical pattern change and it is not surprising that several intermediate runs, under a sudden reduction in pressure, changed from bubble flow in the initial section to slight slugging flow in the second section. It is believed that this shift in pattern, then, was not a result of the disturbance but rather of the pressure drop. The pattern observations tend to confirm, in general, Baker's region of transition between bubble and slug flow.

It may be noticed in Table II (in Appendix A) that in the bubble-flow regime, f/f_L was approximately the same both upstream and downstream of the bend. This was not true, however, outside the bubble regime. For some flows in this category f/f_L was substantially smaller in the upstream test section. The exact cause of this phenomenon is unknown. Several possibilities exist. One is that the pressure being materially different upstream and downstream of the bend, a different pattern of flow occurred (perhaps approaching separated flow) in the upstream section even though this was not apparent in the viewing section which was located at the end of this test section. Another possibility is that the flow pattern actually changed in the upstream test section, perhaps not having settled down to an established pattern at the beginning of the test section. Because of the uncertainty, no attempt has been made to analyse these data at this time.

Using the second apparatus, some data were taken of the pressure drop around the 180-degree bend. The data showed considerable scatter, but the bend coefficient defined as the pressure drop in the bend divided by the dynamic head of the flowing mixture was roughly constant as it is for pure water. Since only one bend was used, and that under limited conditions, more investigation of loss due to bends is required.

3. Chisholm and Laird Experiments [6]

A recent paper by Chisholm and Laird made available data covering a much wider range of variables than that covered in this project. According to the authors, the studies involved bubble, slug, and annular flows under

essentially atmospheric conditions. However, after studying the data fully, it was found that apparently very few were in the bubble-flow regime and a few more were in the transition from bubble to slug flow. Although Chisholm and Laird used nominal 1-in.-diameter pipes of several roughnesses, only their data for smooth and glavanized pipes were considered.

The Chisholm and Laird data, together with some computed numbers, are reproduced in Table III (in Appendix A). The friction factor f was computed from the measured pressure drop using Eq. (17), even though the mixtures in only a very few of the runs could be considered as homogeneous. Flow pattern observations were not recorded by Chisholm and Laird.

The ratios f/f_L were computed using tabulated values of f_L in the Chisholm and Laird paper. Figure 5 portrays the f/f_L data as contours of constant f/f_L on Baker's flow-pattern diagram. The contour lines in the bubble-flow regime of Fig. 5(b) have been drawn with the aid of data from Tables I and II. Some of the Chisholm and Laird data in the bubble-to-slug flow transition region are also plotted in Fig. 3 for comparison with the present data.

C. Friction Factor for Air-Water Mixtures

The friction-factor data from Tables I, II, and III (in Appendix A) have already been plotted in Figs. 3 and 5 in the form f/f_L as a function of Baker's parameters. The galvanized-pipe data from all three tables seem to be in good agreement with each other where they overlap. For the upper diagrams of Fig. 3, where the flow is almost entirely bubble flow,

$$0.98 < f/f_L < 1.25,$$

the higher values of the ratio occurring at the higher gas-liquid flow ratios. A variation of ± 2 per cent in f/f_L can be explained by experimental error; but the remainder of the rise above $f/f_L = 1.0$ is systematic and possibly results from the fact that $\mu > \mu_L$ and becomes increasingly so as the air-water ratio increases. (It may be possible to calculate μ for the mixture from these data.)

Figure 5 gives a picture of the general trend of f/f_L outside the bubble-flow regime. Even though the homogeneous assumption and the assumption of constant Reynolds number used in developing Eq. (17) no longer hold, the

concept of friction factor appears to be a useful one for calculating pressure drop. Both the smooth- and galvanized-pipe data of Chisholm and Laird, when plotted as the ratio f/f_L, exhibit quite similar trends, f/f_L being relatively constant in bubble flow and decreasing steadily and with increasing rapidity as the stratified portion of the diagram is approached. Outside the bubble-flow regime, f/f_L appears to be slightly larger in the galvanized pipe than in the smooth pipe, other conditions being the same. Perhaps a better reference friction factor than f_L could be devised for the Chisholm and Laird data, but no attempt has been made to do so in preparing this paper. Also, Baker's diagram may not be the best base on which to plot these data, especially in view of the presence of the empirical parameters λ and ψ. Some data should be obtained with other pipe sizes to check the method of presentation. Further work toward improving Baker's diagram and correlating friction factor with it may be useful.

In any event, it appears that there is a smooth change in friction factor with the flow parameters even across the transition regions between the various flow patterns. Therefore, a knowledge of the flow pattern does not appear to be essential in predicting f/f_L or pressure drop (within a certain margin of error). The same assumption regarding pressure drop was made in reaching the Lockhart-Martinelli correlations [4].

In view of the approximate independence of f/f_L from flow pattern, it may be possible to find a single parameter which will correlate f/f_L for use in predicting pressure drop. Several parameters have been tested with this object in mind, and the best one appears to be the compressibility parameter θ defined by Eq. (15) and already appearing in the pressure-drop equation, Eq. (17). In Fig. 6 all the data from Tables I, II, and III (in Appendix A) have been plotted in the form of f/f_L versus θ. Figure 6(a) shows these data for $\theta \leq 3$ using a natural scale for θ while Fig. 6(b) shows the data for $\theta \geq 1$ using a logarithmic scale for θ in order to accommodate the wide range of the data.

For Fig. 6(a), where all the data lie within the bubble-flow regime,

$$f/f_L \approx 1 + 0.035 \sqrt{\theta} \qquad (23)$$

fits all the data within ± 4 per cent. This is as close as f_L itself can

be predicted. When extended to the higher values of θ shown on Fig. 6(b), Eq. (23) still fits all the data within about ± 10 per cent to $\theta = 20$. Equation (23) has been plotted on Fig. 6.

At still greater values of θ, f/f_L values decrease again as shown in Fig. 6(b) to a minimum near $\theta = 10^5$ and then appear to rise again. Both the galvanized- and smooth-pipe data of Chisholm and Laird for several values of air-water flow ratio appear to be correlated by the plotting shown in Fig. 6(b). It may be noted that the spread in f/f_L at any θ is not any worse than the spread in pressure drop given by the Lockhart-Martinelli correlations for one pipe surface only, using the same data [6]. The form of plotting used in Fig. 6 needs to be checked using data for other pipe sizes at large θ; such checking is not within the scope of this paper. At the lower values of θ, however, especially in the bubble-flow regime, the plotting used in Fig. 6 has correlated data for several pipe sizes obtained by different investigators and the correlation may be considered quite satisfactory.

It may be observed in Fig. 6(b) that there is a transition between rising f/f_L for $\theta < 35$ and falling f/f_L beyond; and that the transition is near the transition from bubble flow to slug flow. In the present experiments bubble flow always existed for $\theta < 6$. Slug flow always existed for $\theta > 45$. In the intermediate region, the flow could be either essentially bubble or slug flow, depending on other parameters. There is a possibility that the transition in slope of f/f_L is related to the change in flow pattern.

IV. ANALYSIS AT A CROSS SECTION

A. Phase Fraction and Phase Velocity

1. Homogeneous and Nonhomogeneous Flow

Liquid and gas fraction have been defined by Eq. (6) and liquid and gas velocities by Eq. (7) of Section II. The relation between these equations was given by Eq. (8),

$$R_G/R_L = V_L/(\pi V_G) \tag{8}$$

For steady bubble flow (and perhaps for steady mist flow) in horizontal pipes where the mixture may be considered pseudo-homogeneous, $V_G \approx V_L$

since the gas bubbles are trapped in the surrounding liquid flow (or the mist droplets are trapped in the surrounding gas flow). Then Eq. (8) becomes

$$R_G/R_L \approx 1/\pi \tag{24}$$

This is the basic equation for phase fraction when the flow can be assumed homogeneous.

In nonhomogeneous flow patterns, it is not so simple to predict the relation between V_G and V_L. In annular flow, where the gas component is completely isolated from the pipe walls by the liquid component, $V_G > V_L$. In separated and slug flow it is not possible to make a definite statement without further information, but because of direct wall friction of the gas in these cases it is unlikely that the ratio V_G/V_L will ever exceed that for annular flow. Hence, as the gas flow rate increases at constant water flow rate, it can be surmised that V_G/V_L will rise from near unity for bubble flow, reach a crest for annular flow, and recede toward unity for mist flow. Corresponding changes in R_G/R_L in accordance with Eq. (8) can be expected.

2. Experimental Evaluation of R_G/R_L and V_G/V_L

Phase fraction and velocity measurements were not obtained in the present experiments, but were obtained by Chisholm and Laird [6] in connection with the friction-factor experiments discussed earlier. They used the method of trapping the flow between two simultaneously closing valves and measuring the liquid fraction. The Chisholm and Laird data for liquid fraction were already tabulated in Table III (in Appendix A), as were the computed results for V_G/V_L.

The two quick-closing valves in the Chisholm and Laird experiments were located 8 ft apart in a 1-in. pipe, so that R_L has been averaged over a reach whose average pressure is not precisely known--only the pressure at the midpoint of the reach is given and this is recorded in Table III in terms of the parameter π as $1/\pi_m$ (where the subscript denotes measurement at the midpoint of the test length).

The Chisholm and Laird data, plotted as log (R_G/R_L) versus log $(1/\pi_m)$ are shown in Fig. 7. Also shown in Fig. 7 is the line of Eq. (24),

the homogeneous flow theory result. The data for both the smooth and galvanized pipes appear to correlate along a fairly well-defined curve that is bounded for small air-water flow ratios by Eq. (24). Furthermore, for large air-water flow ratios (large $1/\pi_m$) the data appear to be limited by another straight line parallel to that given by Eq. (24), indicating that a maximum value of V_G/V_L has been reached.

The velocity-ratio data are plotted on Baker's diagram in Fig. 8. As was the case with friction factor, there appears to be a smooth change in V_G/V_L independently of flow pattern. Again, the smooth- and galvanized-pipe results are qualitatively similar with the velocity ratio somewhat larger for the galvanized pipe than for the smooth pipe, other conditions being the same, except near the bubble-flow regime.

Comparison of Figs. 5 and 8 shows that there is no correlation between f/f_L and V_G/V_L.

The assumption that $V_G/V_L \rightarrow 1$ in the bubble-flow regime appears to be substantially supported by the Chisholm and Laird data.

B. Experiments on Bubble-Size Distribution

1. Apparatus

The apparatus used to measure bubble size in the 2-1/2-in. pipe is shown in Fig. 9. The mixture of air and water is generated as described in Section III. After an appropriate length of run, the mixture passes through the sampler where it is split into two parts. The smaller part passes through a narrow, transparent test section that permits photographic determination of bubble size. The remainder of the flow is turned through a bypass line and rejoins the sampled material immediately behind the test section. The pressure in the transparent section is measured by a manometer in comparison with the pressure just upstream from the sampler.

The pipe-test length consisted of four 5-ft sections of 2-1/2-in. pipe. These lengths were aligned by using predrilled aligning holes in the flanges and snug-fitting aligning pins. The sampler could be installed at either end of the 20-ft test run or at the quarter points. The details of the sampler construction and the techniques used in photographing, sampling, measuring, and counting the bubbles are given in Reference [7].

The same sampler, with appropriate 4-in. fittings, was used for the 4-in. pipe. In this pipe, however, the vertical height of the sampled section consisted only of a half diameter of pipe instead of a whole diameter as in the 2-1/2-in. pipe. Hence, a photograph of a sample would show the bubbles in the upper half or the lower half of the pipe, depending upon which way the sampler was installed. This meant that a nonuniform bubble distribution would cause errors in the size distribution. For this reason the sampler was installed on the 4-in. pipe at the entrance to the first 5-ft section only where the separating process would have the least time to occur. For this report, the samples were taken in the upper half of the 4-in. pipe only.

2. Data and Discussion of Results

In the 2-1/2-in. pipe, sampler data were actually obtained at both ends and at the middle of the test pipe. As for the pressure-drop data discussed in Section III, only small air-water ratios were used ($\theta \leq 1.5$) so that the flow was in the lower part of the bubble regime.

A number of preliminary experiments, not detailed herein, showed that within the limits of experimental error, the bubble-size distribution at the various positions of the sampler were reducible to each other using the perfect gas laws. Hence, all bubble-size data were eventually reduced to atmospheric conditions using the perfect gas laws. Most careful attention was given to counting the bubbles and measuring sizes for the runs with the sampler at the middle of the test pipe. The data for these runs are given in Table IV (in Appendix A) with the designation M following the run number. All of the 4-in.-pipe data are also included in Table IV, the letter A denoting that the runs were taken with the sampler at the beginning of the test length as already noted. Typical data from Table IV are plotted on logarithmic probability paper in Fig. 10(a).

Dimensional analysis indicated that the bubble-size data might be correlated by introduction of a dimensionless bubble diameter d' given by the modified Weber number,

$$d' = V_\ell d \sqrt{\rho_L/(\sigma D)} \tag{25}$$

Here d is the bubble diameter measured at atmospheric conditions and σ is the surface tension of the water. Computed values of d' are given in Table IV and plotted in Fig. 10(b) on semilogarithmic paper for both the 2-1/2-in. and 4-in. pipe. Although the data scatter somewhat, a mean line can be drawn through the data; the equation of this line is:

$$d' = 7.50 - 1.49\ \ell n \quad \text{(per cent larger)} \tag{26}$$

For the 50 per cent size, which may be called the geometric mean size and labeled d_{50}, the straight line of Fig. 10(b) gives $d' = 1.67$. Using this value (together with the numerical values $\rho = 1.94$ and $\sigma = 0.005$ in the pound-foot-second system) in Eq. (25) yields

$$d_{50} = \sqrt{D/V_\ell} \propto \frac{\sqrt{D}}{(G_L/A)} \tag{27}$$

Direct measurements of d_{50} for each run from graphs like those in Fig. 10(a) have been plotted in the form of Eq. (27) in Fig. 11 and compared with the equation. The scatter of data in Fig. 10(b) shows up as a deviation from Eq. (27) in Fig. 11, but there is a very definite trend for mean bubble size to increase with the square root of the diameter of the pipe and inversely as the liquid flow rate per unit area. This means that as the slug-flow regime in Fig. 1 is approached, the bubbles increase in size, and vice versa.

The data in Table IV (in Appendix A) as typified by Fig. 10(a), indicate that there is little variation in size distribution. The bubble diameter exceeded by only 5 per cent of the bubbles, d_5, has also been plotted on Fig. 11 as a function of $\sqrt{D/V_\ell}$. It is seen that these large bubbles have approximately three times the diameter of the mean bubbles. The range of variables in the present investigation has been quite small, however. A wider range might bring new factors to light.

C. Velocity Traverses in Bubble Flow

1. Apparatus and Data

Both the 2-1/2-in. and 4-in. test pipes used in the pressure-drop experiments of Section III were provided with velocity-probe stations at or near the positions of the downstream pressure taps shown in Fig. 2. A Pitot cylinder was used as a measuring probe for the total head. Each station consisted of two pairs of holes drilled in the pipe wall, the holes of each pair being at opposite extremities of a vertical or horizontal diameter. The Pitot cylinder passed through both holes of a pair; in the 4-in. pipe the cylinder could be traversed across the pipe from wall to wall, but in the 2-1/2-in. pipe, it was possible to traverse only from the wall to the center. In the

2-1/2-in. pipe a 0.075-in. OD cylinder was used, while in the 4-in. pipe, the cylinder was 0.125-in. OD. Traversing was by screw thread, the least reading in the smaller pipe being 1/80 in. and in the larger pipe, 1/96 inch. The stagnation hole in each cylinder was a No. 76 drill hole (0.020 in.).

Static head was measured at the pipe wall opposite the Pitot cylinder by manifolding the two probe holes not in use for the cylinder. Static head and total head were compared in a mercury U-tube manometer to read velocity head. Before and after each traverse, the static-head readings were compared with the static head at an upstream ring of taps, with the Pitot cylinder both in and out of the flow. The information so obtained was used to correct the measured velocity head to the value it would have had without the blockage caused by the presence of the Pitot cylinder.

A few velocity-head measurements were made for small air-water flow ratios using this apparatus. Velocity head was determined in exactly the same manner for both pure water flows and air-water mixture flows. In the mixture flows, no bubbles entered the stagnation hole of the Pitot cylinder because of the curved streamline pattern around the cylinder. Occasionally, bubbles entered one of the manifolded static lines (transparent tubing was used for these lines so that bubbles could be observed); when this occurred, the lines were flushed before proceeding with the experimental work. Actually, the velocity head of the water phase of the misture was measured by the process described, but it was already known from the analysis of Part A preceding, that the entrained bubbles moved at approximately the same mean speed as the water. Hence, it was assumed that the measured velocity head and the velocity derived therefrom was applicable to the mixture as a whole. Integration of the velocity profiles and comparison with the measured input of air and water, as shown subsequently in Table VII, indicated that there was some error in this assumption; however, the error is probably unimportant insofar as the purposes to which the profiles will be put are concerned.

Four different sets of velocity data were obtained, two sets in the 4-in. pipe and two in the 2-1/2-in. pipe. Table V lists the general flow properties associated with each of the runs. In every case, each diametral or radial traverse in the air-water mixture was preceded by a similar traverse in pure water. The Pitot cylinder was not withdrawn between these pairs of traverses. This procedure permitted the zero of the tube in the mixture

flow to be well established, as will be demonstrated below. Velocity profiles for the air-water mixture flows are plotted in Fig. 12. In the figure, y is the distance from the pipe wall, and r is the radius of the pipe.

TABLE V

FLOW PROPERTIES FOR VELOCITY TRAVERSES

Run	Pipe Dia. in inches (nominal)	Flow Rate Water Only cfs	Air-Water Mixture						
			Measured Flow Rate			G_G/A lb/sec ft^2	α x 10^3	$1/n$	λ
			Water cfs	Air* cfs	Total cfs				
I	4.0	1.861	1.740	0.198	1.938	0.28	0.229	0.114	1.29
II	4.0	1.850	1.730	0.256	1.986	0.39	0.320	0.148	1.34
III	2.5	0.805	0.679	0.128	0.807	0.52	0.407	0.189	1.34
IV	2.5	0.860	0.806	0.335	1.141	1.09	0.720	0.415	1.20

*Converted to probe-station conditions using the perfect gas law.

2. Analysis and Discussion of Results

It is immediately apparent from Fig. 12 that the velocity distribution is materially affected by the presence of the air bubbles, particularly near the top of the pipe. (Similar profiles for the pure-water runs show about the same scatter as is shown between the horizontal traverse points of Fig. 12.) In particular, at the higher air concentrations, the velocity distribution in the vertical is asymmetrical, while that in the horizontal is as symmetrical as in the case of pure water. The velocity profiles in the upper vertical traverses are generally not so flat as those in the other traverses; this would indicate that the pipe with air-water mixture flow is effectively rougher near the top than elsewhere. It is to be expected that there will also be lack of symmetry of the wall-shear stress distribution and, perhaps, secondary currents in the mixture.

In order to investigate the wall region in air-water mixture flows more completely, the data leading to Fig. 12 were replotted using a logarithmic scale for the wall distance. The replotted data are shown in Fig. 14, while corresponding data for pure-water flows are shown in Fig. 13.

The zero of the wall-distance scale in these figures is not a measured value, but lies somewhere within the rough-pipe surface. The origin

was determined from the pure-water traverses for each run by assuming that there exists a universal law of the wall of the form [10].

$$V = aV_* \log y + bV_* \tag{28}$$

where V is the local velocity,

$V_* = \sqrt{\tau_o/\rho}$ is the shear velocity,

τ_o is the wall-shear stress,

ρ is the fluid density,

y is the distance from the wall,

a is a universal constant given as 5.6 by Clauser [10], and

b is a lumped constant including the roughness effect of the walls and depending on the units used for other terms.

The law, Eq. (28), was assumed to hold from very near the wall toward the center as far as a value of y of 15 or 20 per cent of the pipe radius. By uniformly increasing or decreasing the values of y read on the Pitot-cylinder scale until the points approached as closely as possible to satisfying Eq. (28), the pure-water traverses shown in Fig. 13 were obtained. The effective diameter of the 4-in. pipe between virtual zeros turned out to be considerably greater than the measured diameter between roughness tips, as shown in Table VI.

TABLE VI

DIAMETER OF 4-INCH PIPE

	Measured by Calipers	Distance Between Virtual Origins	
		Run I	Run II
Vertical, in.	4.036	4.077	4.066
Horizontal, in.	4.000	4.097	4.076

Also obtainable from Fig. 13 are values of the shear velocity, V_*. For pure-water flows, the shear velocity is related to the friction factor, f, by Eq. (13a) which may be written

$$f_L = 8(V_*/V_L)^2 \qquad (29)$$

The values of f_L obtained from V_* in Fig. 13 using the value 5.6 for a in Eq. (28) are shown in Table VII and compared with the corresponding values from pressure-drop measurements obtained further upstream. The friction factors by the velocity traverses appear to be generally greater than those by pressure drop. The difference may be real because of the different measuring locations.

Having determined the virtual origin for each traverse from the pure-water data, the same origin was used for the corresponding air-water mixture traverse, (which, as already noted, was taken immediately after the pure-water traverse without withdrawing the tube). The air-water mixture graphs of Fig. 14 were obtained from Fig. 12 by this means. It may be observed that there is a strong tendency for the air-water mixture profiles to follow Eq. (28) near the wall, also, albeit with different values of the coefficients aV_* and b than for pure water.

TABLE VII

RESULTS OF VELOCITY TRAVERSES

Run	Integrated Flow Rates				Friction Factor Water Only, f_L		f/f_L Air-Water Mixture	
	Water Only cfs	% Diff. from Measured	Air-Water Mixture					
			Total cfs	% Diff. from Measured	Pressure Drop*	Vel. Trav.	Pressure Drop**	Vel. Trav.
I	1.866	+0.3	1.910	-1.4	0.0144	0.0178	1.00	1.046
II	1.792	-3.1	1.896	-4.5	0.0144	0.0151	1.01	1.026
III	0.790	-1.9	0.772	-4.3	0.0186	0.0178	1.02	1.013
IV	0.840	-2.3	1.054	-7.6	0.0178	0.0198	1.06	1.009

*Computed from measured pressure drop between the two upstream stations shown in Fig. 2.

**Average values from Fig. 3.

That the air-water mixture traverses follow the law of Eq. (28) is not surprising if it can be assumed that a bubbly mixture at small air-water ratios is locally homogeneous in the wall region of each traverse. Assuming that Eq. (28) applies, a value for V_* can be determined from the slopes of

the straight lines for each traverse if a is assumed constant (at, say, 5.6). It is readily seen from Fig. 14 that aV_*, and hence the wall-shear stress, is generally greatest near the top of the pipe and least near the bottom. This result appears somewhat anomalous; it might, at first, be expected that the presence of air would tend to reduce the shear stress as in the central parts of the pipe. To explain the wall-shear-stress distribution around the periphery of the pipe, it may be conjectured that there is a secondary current flowing from the center toward the top, down around the sides to the bottom, and thence up to the center. Such a current would tend to thin the viscous region near the top and thicken it near the bottom of the pipe, thus increasing the effective roughness near the top and decreasing it near the bottom. Increased effective roughness near the top of the pipe is in accord with the velocity profiles of Fig. 12.

The ratio f/f_L may be determined from Figs. 13 and 14. If in pure liquid, the measured slopes of the straight lines representing the velocity traverses in Fig. 13 are designated as $aV_* = S_L$, while in the mixture, the average of the measured slopes is designated as $\overline{aV}_* = S_M$, the following relations apply:

$$\overline{\tau_o} = \overline{\rho V_*}^2 = \overline{\rho}(S/a)^2 \tag{30}$$

$$f_L = \frac{8\,\tau_{o,L}}{\rho_L V_\ell^2} = \frac{8(S_L/a)^2}{V_\ell^2} \tag{31}$$

$$f = \frac{8\,\tau_{o,M}}{\rho V^2} = \frac{8(S_M/a)^2}{V_L^2\,(1 + 1/\pi)^2} \tag{32}$$

$$f/f_L = [(S_M/S_L)(V_\ell/V_L)(1/(1 + 1/\pi))]^2 \tag{33}$$

Friction-factor ratios have been computed from the data in Figs. 13 and 14 using Eq. (33), and the results are shown in Table VII; comparison is made with the pressure-drop results from Fig. 3. Numerically, the comparison is probably

as close as can be expected; the trends of the data appear to be in opposite directions, however.

In Fig. 15 the velocity traverses for Run IV of Fig. 14 have been replotted in the more conventional form

$$V/V_* = a \log yV_*/\nu + b' \tag{34}$$

and compared with an accepted formula for smooth boundary-layer flow. Also shown is one of the pure-water traverses for Run IV from Fig. 13. It appears that the bottom of this galvanized pipe behaves like a smooth surface while the top acts like a pipe of increased roughness in the presence of air bubbles. The conjecture on secondary currents offered earlier would seem to explain the relative locations of these curves.

The large discrepancy in integrated air-water flow rates for Run IV as shown in Table VII could be reduced by taking $V_G/V_L > 1$ in the integration. For $V_G/V_L = 1.22$, for example (which appears reasonable from Fig. 8(b)), the percentage error would be the same as for the pure-water flow.

V. SUMMARY AND CONCLUSIONS

In bubbly mixtures flowing in horizontal pipes, it has been shown that pressure drop may be calculated by using the conventional friction factor for flow of a homogeneous fluid in the pressure-drop equation, Eq. (17).

$$\frac{fx_1}{2D} = \theta(\pi_o - \pi_1) - \ell n \frac{\pi_o}{\pi_1} \left(\frac{\pi_o + 1}{\pi_1 + 1} \right)^{\theta-1} \tag{17}$$

In order to obtain the friction factor f, the Reynolds number and pipe roughness must be known. As a rough approximation,

$$f = f_L$$

where f_L is the friction factor for the liquid component of the mixture flowing alone in the given pipe. The present experiments show that a somewhat better estimate for f can be obtained using the empirical relation given by Eq. (23)

$$f/f_L = 1 + 0.035 \sqrt{\theta} \qquad (23)$$

Equation (23) indicates that the friction factor is actually increased by the presence of bubbles. The increase is possibly attributable to an increase in viscosity.

Whether or not bubble flow occurs depends on the gas-liquid flow ratio and on the liquid or gas flow rate per unit area. Baker's diagram reproduced in Fig. 1 might be used for estimating the limits of the bubble-flow regime. From the diagram it appears that bubble flow will occur only for water flow rates greater than about 500 lb/ft^2-sec. This limit has been verified roughly in the present experiments. The present experiments showed that bubble flow always existed for $\theta < 6$ and essentially bubble flow might exist for θ as great as 45.

Outside the bubble regime, Eq. (17) is still useful for calculating pressure drop. However $f < f_L$, generally. Figures 5 and 6 give some information regarding the ratio f/f_L for these flows, but more study is required before a general rule for finding f can be given. It appears that flow pattern, in itself, is of little importance in predicting f.

In the bubble regime, the bubbles move at approximately the same speed, or very slightly faster than the mean liquid velocity. In other regimes, the gas component moves faster than the liquid, the mean velocity ratios reacing a maximum in annular flow. Again, flow pattern outside the bubble regime has little direct influence on relative liquid and gas velocity.

The velocity profiles in bubble flow in a horizontal pipe are quite similar to those in flow of a single fluid. However, the profiles are not symmetrical about the pipe axis; the profiles seem to indicate a secondary current upward in the center of the pipe and downward around the walls. The upper part of the pipe, where the bubbles are more concentrated, is effectively rougher than the bottom.

Bubble size in bubble flow is proportional to the square root of the pipe size and inversely to the liquid flow rate per unit area. The bubbles become larger as the flow goes from the bubble-flow pattern toward the slug-flow pattern.

As a tentative conclusion, it appears that disturbances of the flow, such as produced by bends, do not alter the conclusions already given above; the pressure drop is given by Eq. (17) on both sides of the bend, proper values of the parameter π being used on each side. The effect of disturbances of other types is still under study.

LIST OF REFERENCES

[1] Santalo, M. A. "Two-Phase Flow." Applied Mechanics Reviews, Vol. 10, pp. 523-526. 1958.

[2] Baker, O. "Simultaneous Flow of Oil and Gas." Oil and Gas Journal, Vol. 53, No. 12, pp. 185-195. July 26, 1954.

[3] Boelter, L. M. K., Martinelli, R. C., Morris, E. H., Taylor, T. H. M., and Thomsen, E. G. "Isothermal Pressure Drop for Two-Phase, Two-Component Flow in a Horizontal Pipe." Transactions of the American Society of Mechanical Engineers, Vol. 66, pp. 139-151. 1944.

[4] Lockhart, R. W., Martinelli, R. C., and Putman, J. A. "Two-Phase, Two-Component Flow in the Viscous Region." Transactions of the American Institute of Chemical Engineers, Vol. 4, pp. 681-705. 1946.

[5] Lockhart, R. W., and Martinelli, R. C. "Proposed Correlation of Data for Isothermal Two-Phase, Two-Component Flow." Chemical Engineering Progress, Vol. 45, pp. 39-48. 1949.

[6] Chisholm, D., and Laird, A. D. K. "Two-Phase Flow in Rough Tubes." Transactions of the American Society of Mechanical Engineers, Vol. 80, No. 2, pp. 276-286. February 1958.

[7] Silberman, Edward, and Ross, James A. Generation of Air-Water Mixtures in Closed Conduits by Aspiration. University of Minnesota, St. Anthony Falls Hydraulic Laboratory Project Report No. 43, December 1954. (Available only on University inter-library loan.)

[8] Schlicting, H. Boundary Layer Theory. New York: McGraw-Hill Book Company, 1955.

[9] Weining, F. S. "Some Properties of Foam and the Possible Use of Foam for Model Tests Especially in Hypersonic Range." Proceedings, Third Mid-Western Conference on Fluid Mechanics, University of Minnesota, pp. 515-527. 1953.

[10] Clauser, F. H. "The Turbulent Boundary Layer." Advances in Applied Mechanics, IV, New York: Academic Press, pp. 1-51. 1956.

F I G U R E S

(1 through 15)

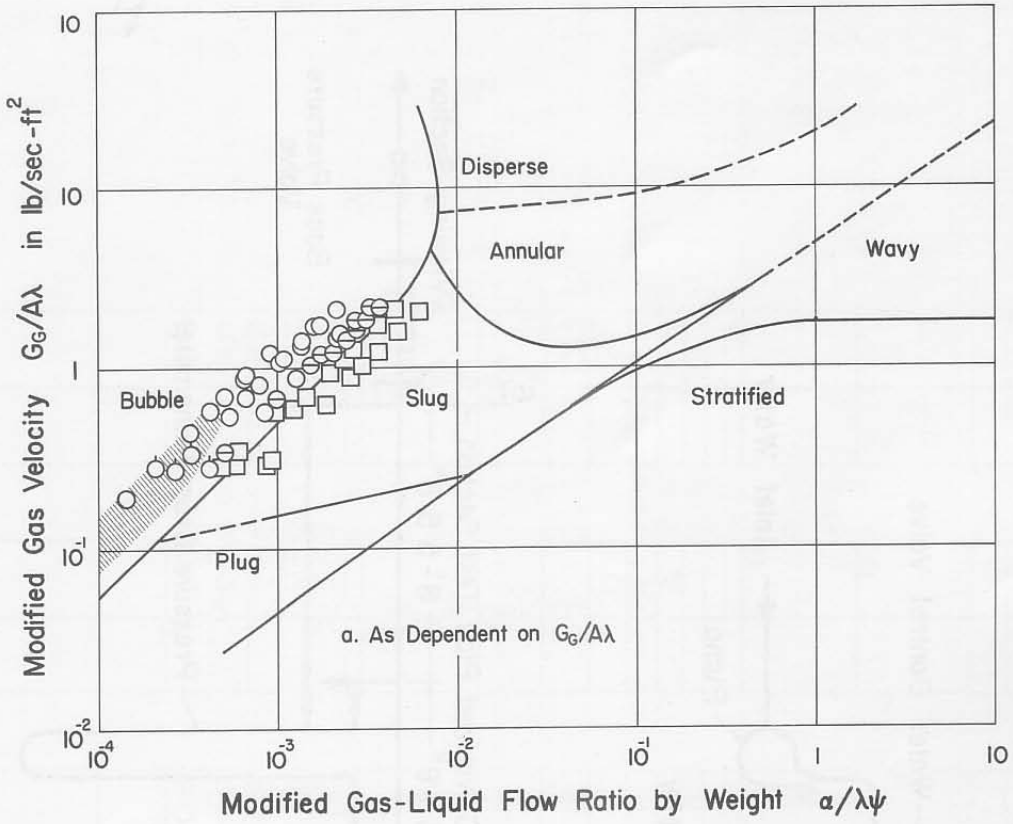

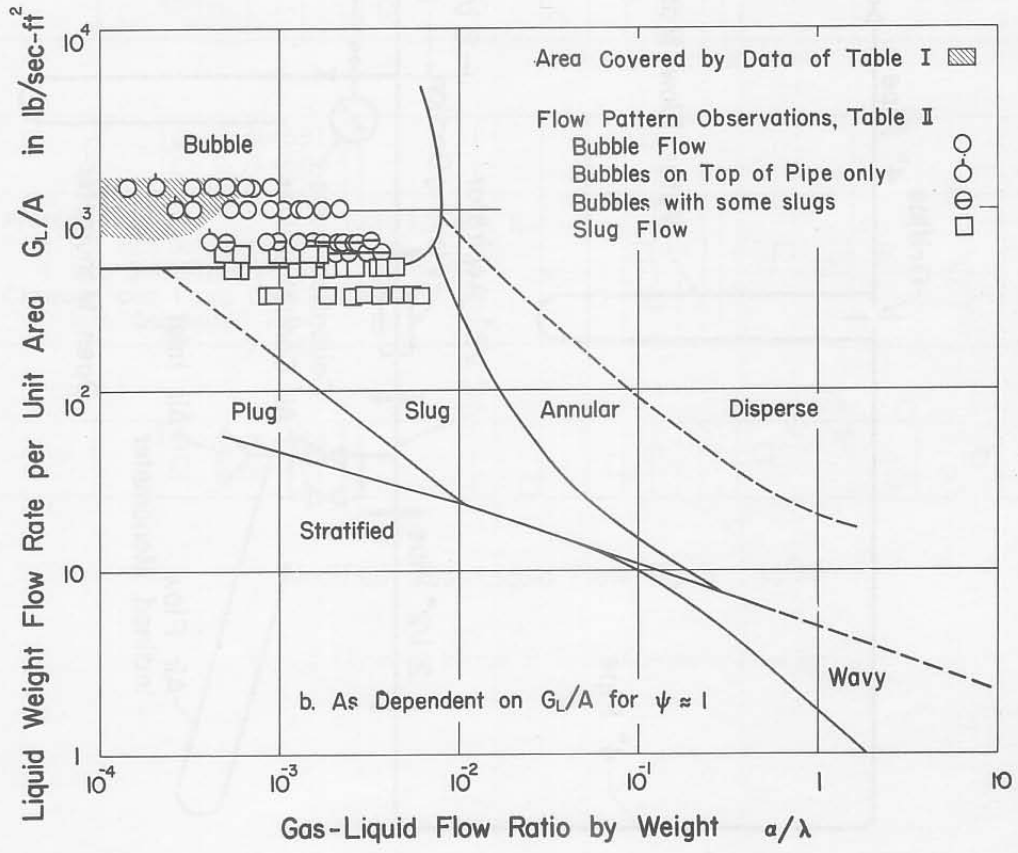

Fig. 1 - Flow-Pattern Regions

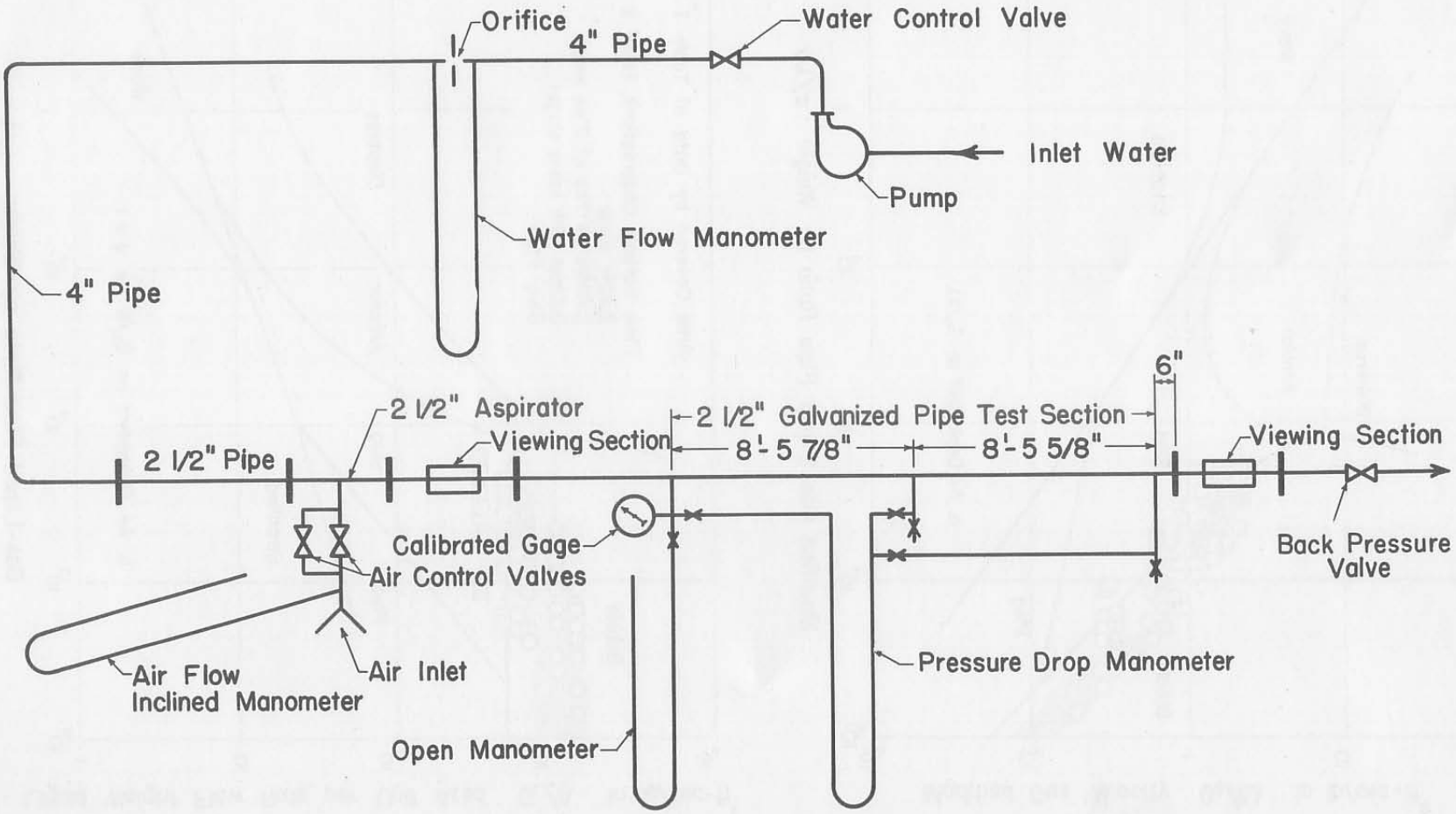

Fig. 2 - Schematic Drawing of First Experimental Apparatus

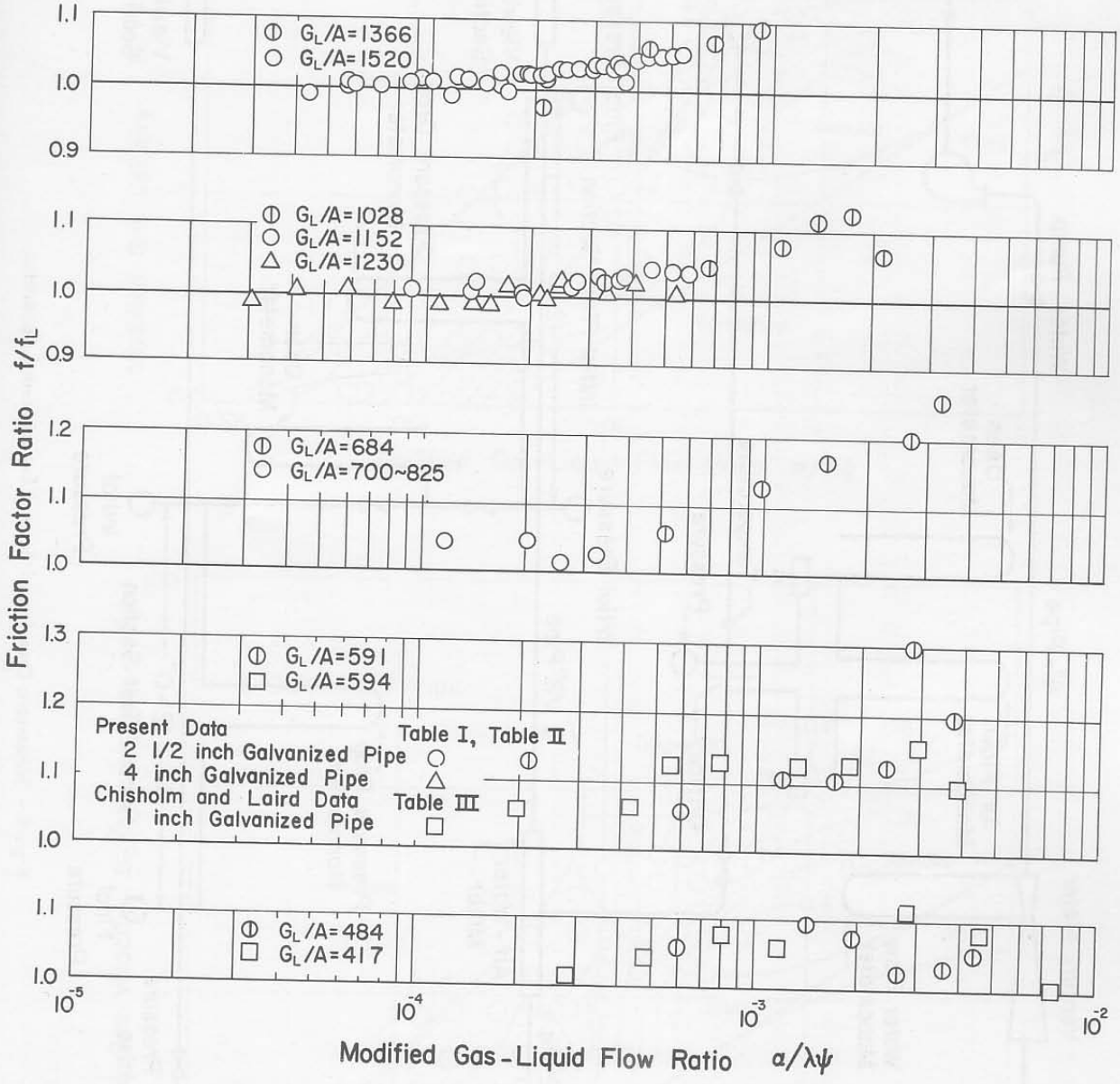

Fig. 3 - Friction Factor at Small Air-Water Flow Ratios

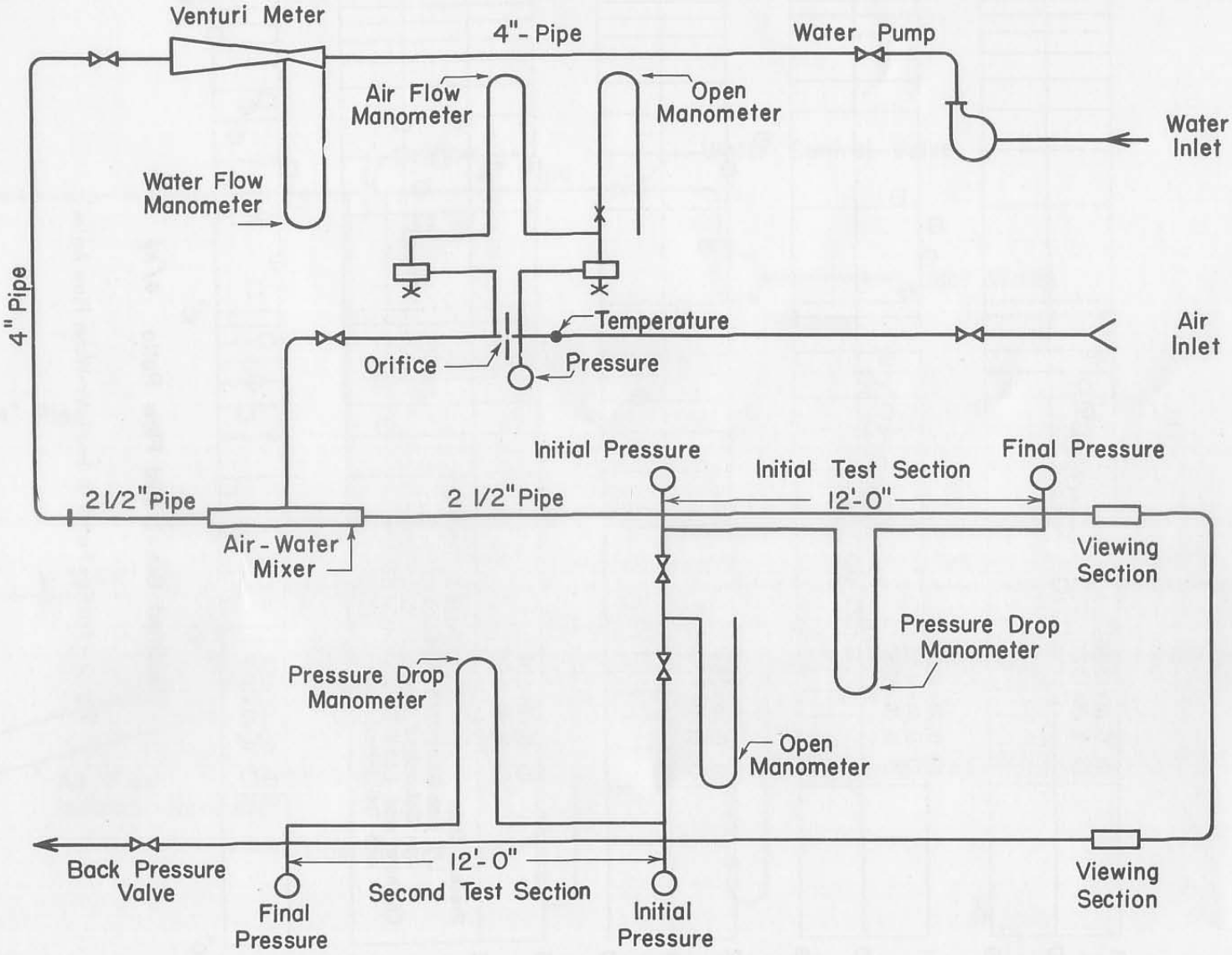

Fig. 4 - Schematic Drawing of Second Experimental Apparatus

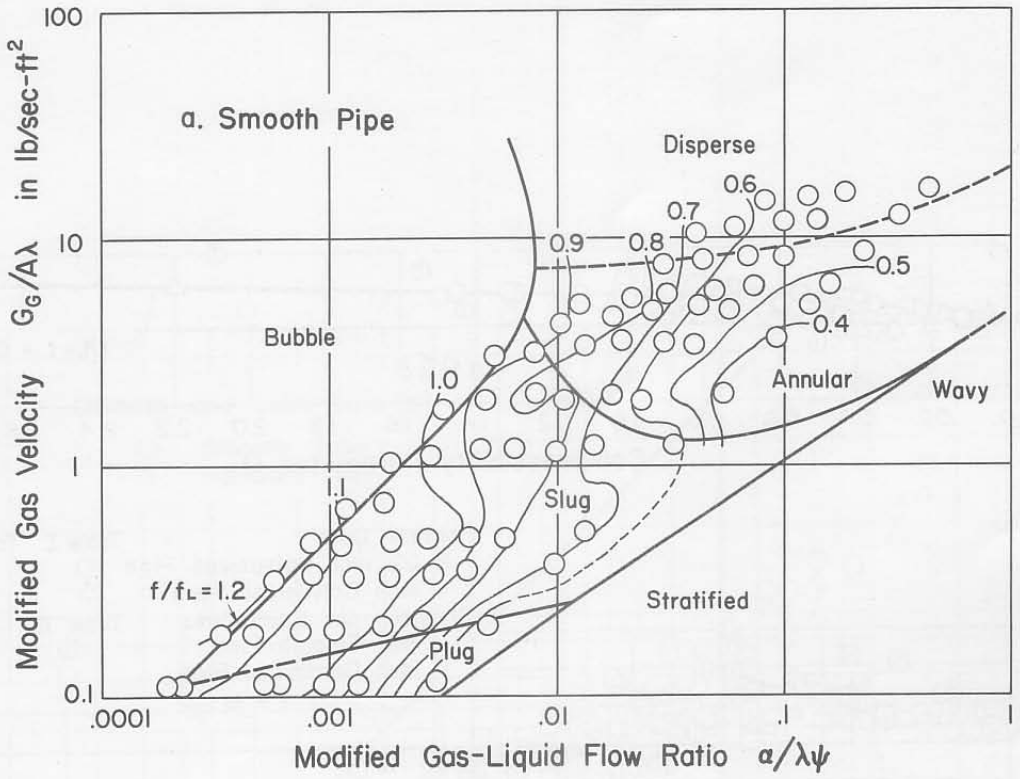

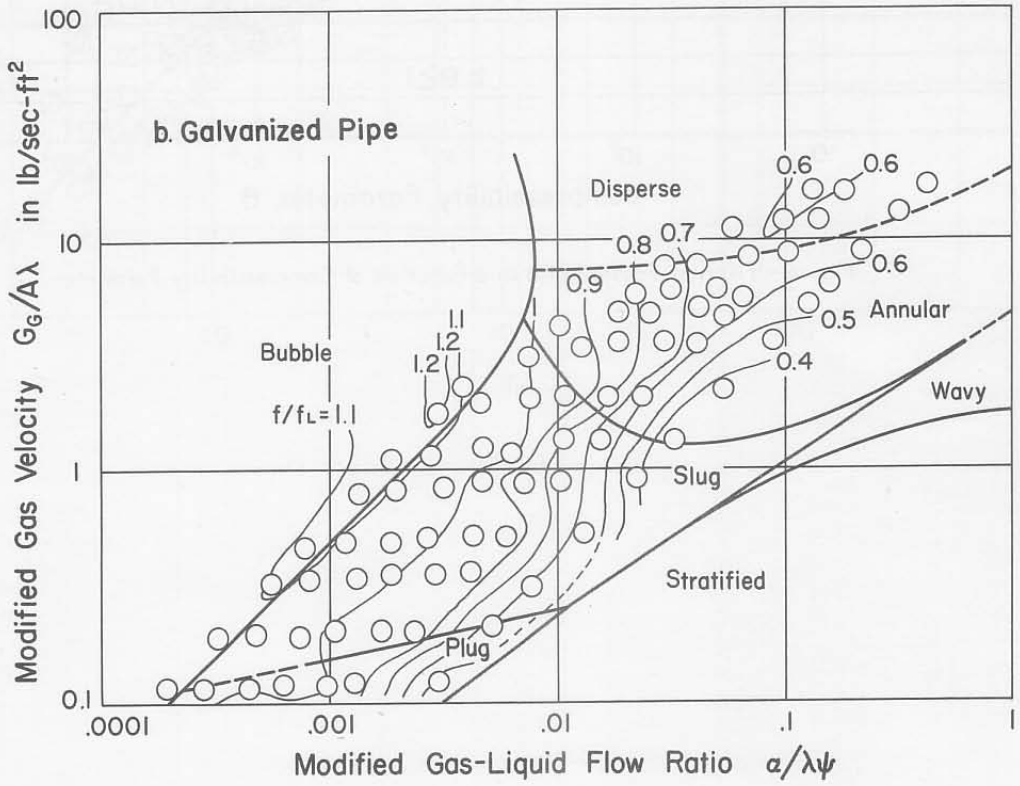

Fig. 5 - Chisholm and Laird Friction-Factor Data

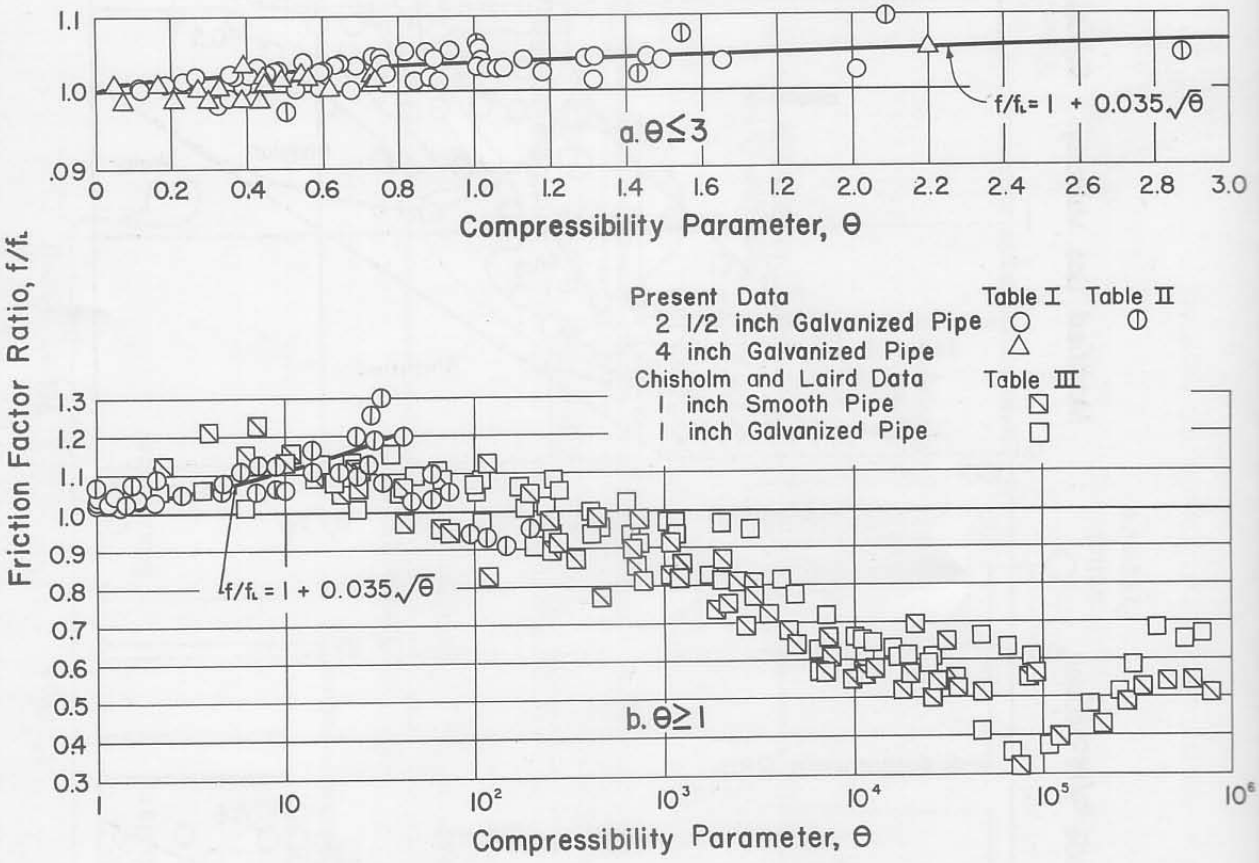

Fig. 6 - Friction-Factor Ratio as a Function of Compressibility Parameter

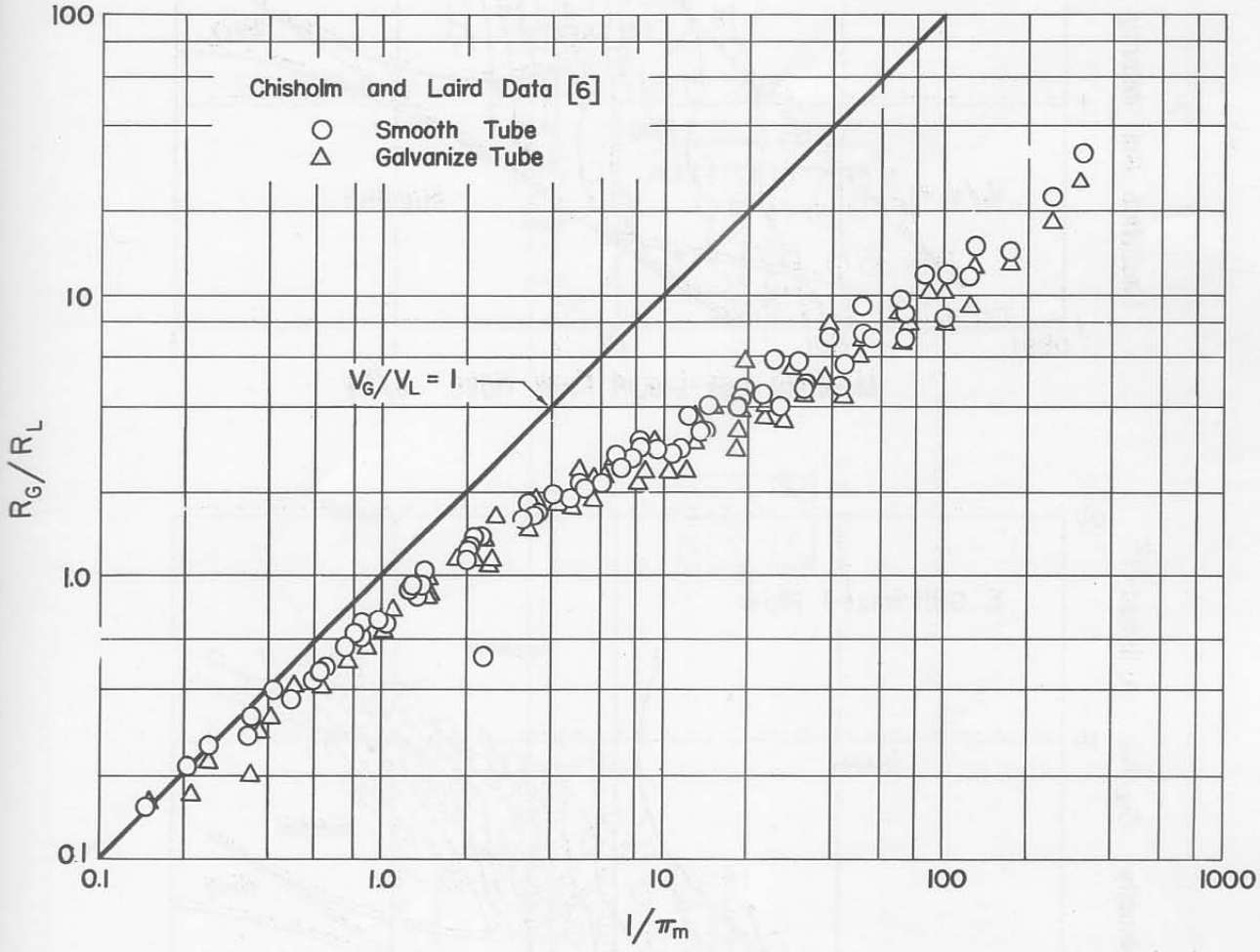

Fig. 7 - Gas-Liquid Fraction

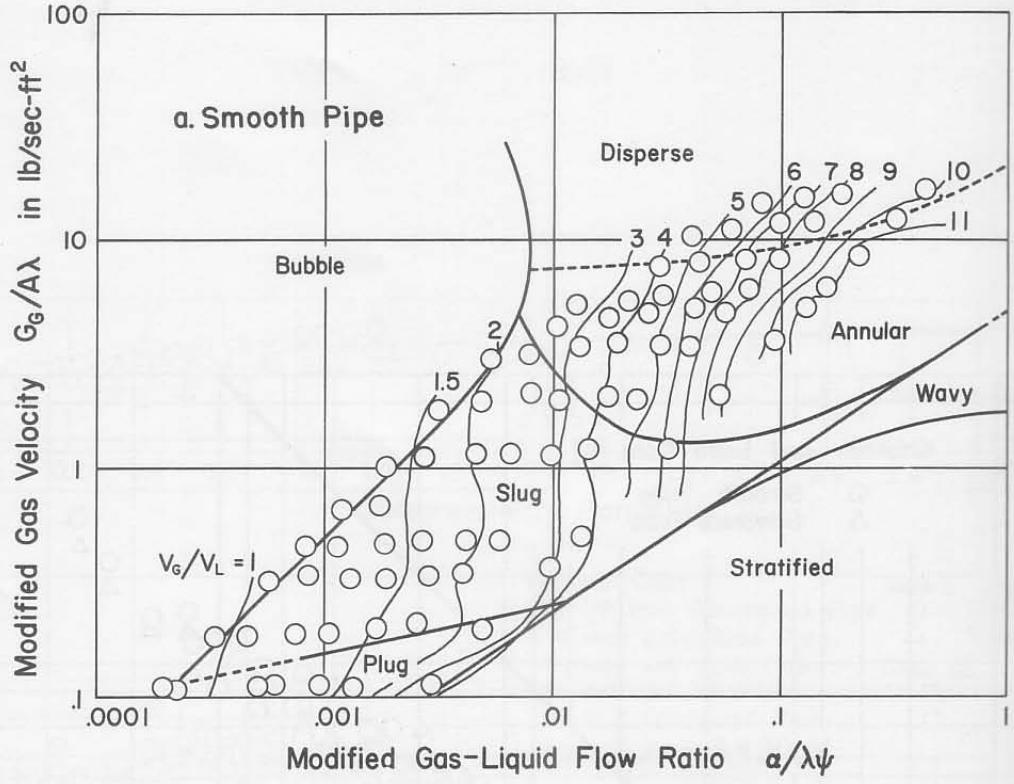

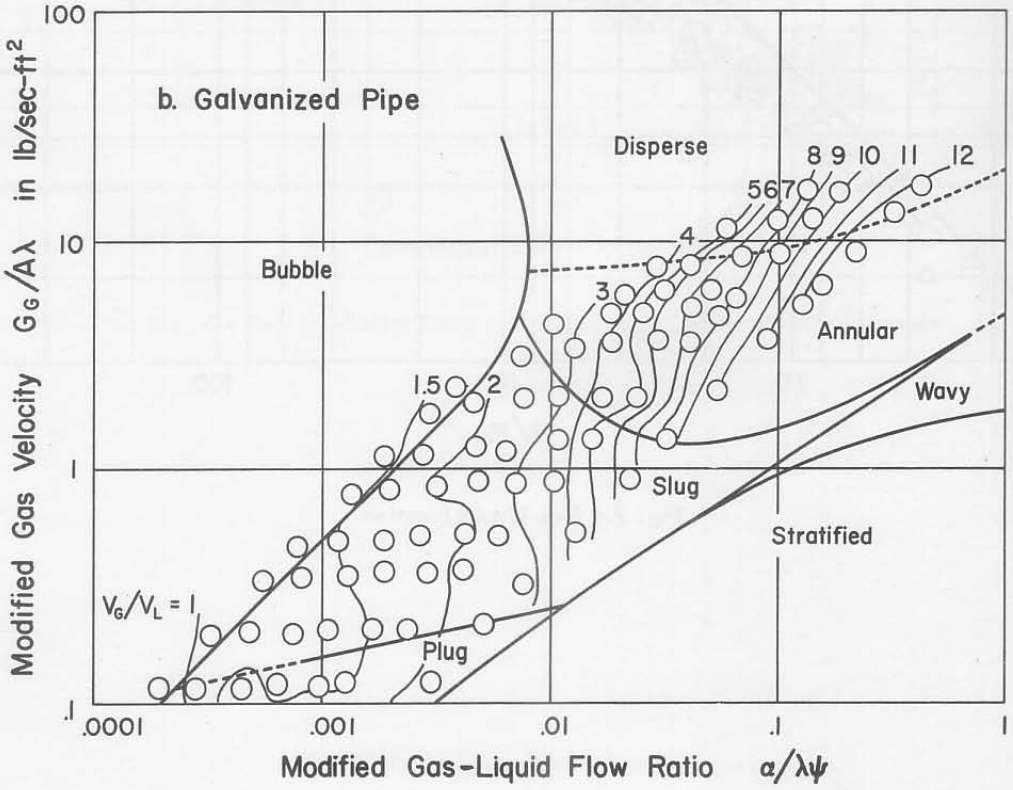

Fig. 8 - Velocity Ratio from Chisholm and Laird Data

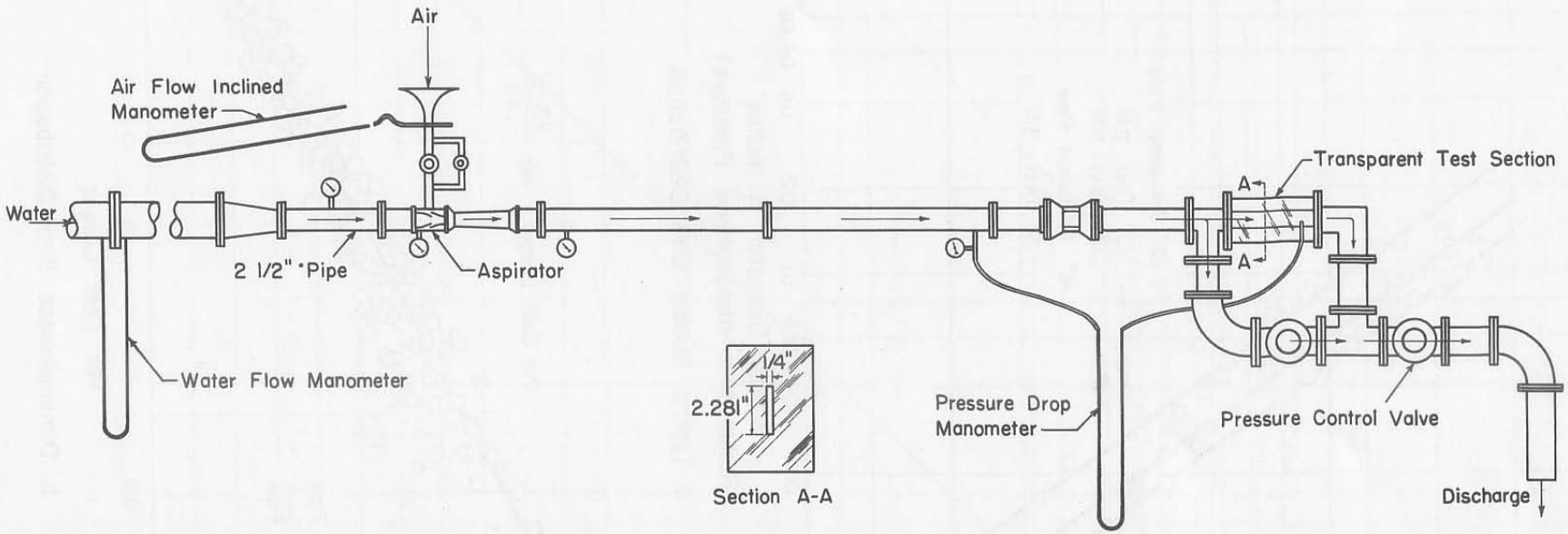

Fig. 9 - Sampling Apparatus for Bubble Size

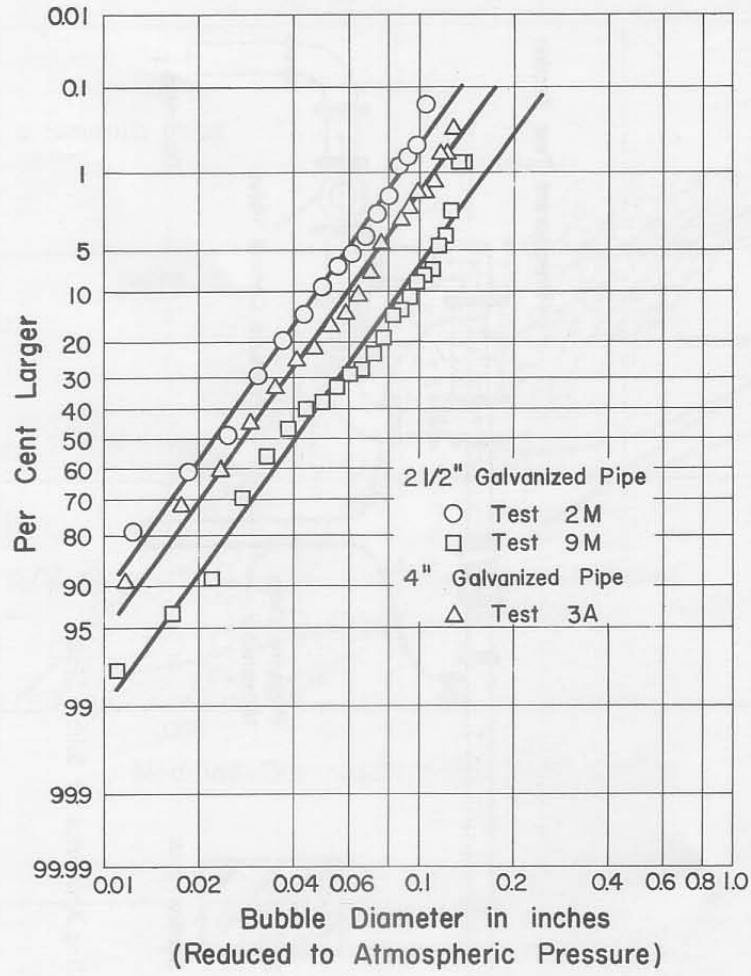

a. Typical Bubble Size Distribution

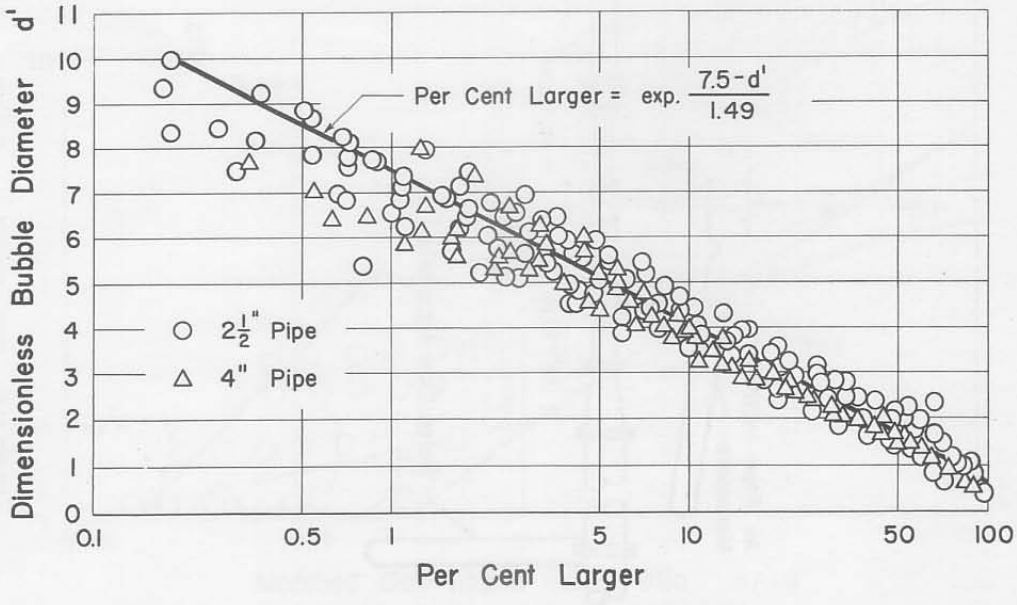

b. Dimensionless Size Distribution

Fig. 10 - Bubble-Size Distribution

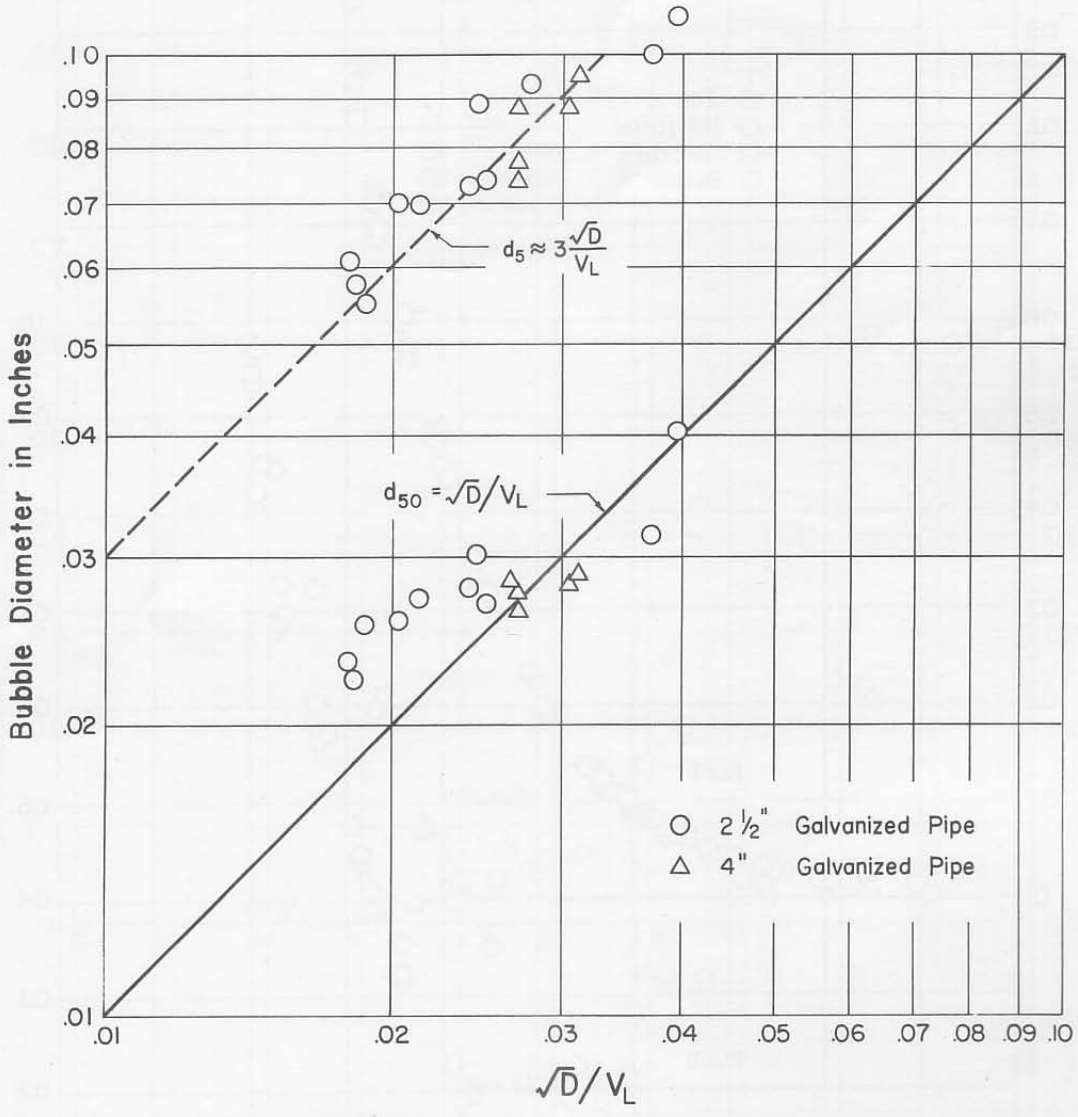

Fig. 11 - Characteristic Bubble Size

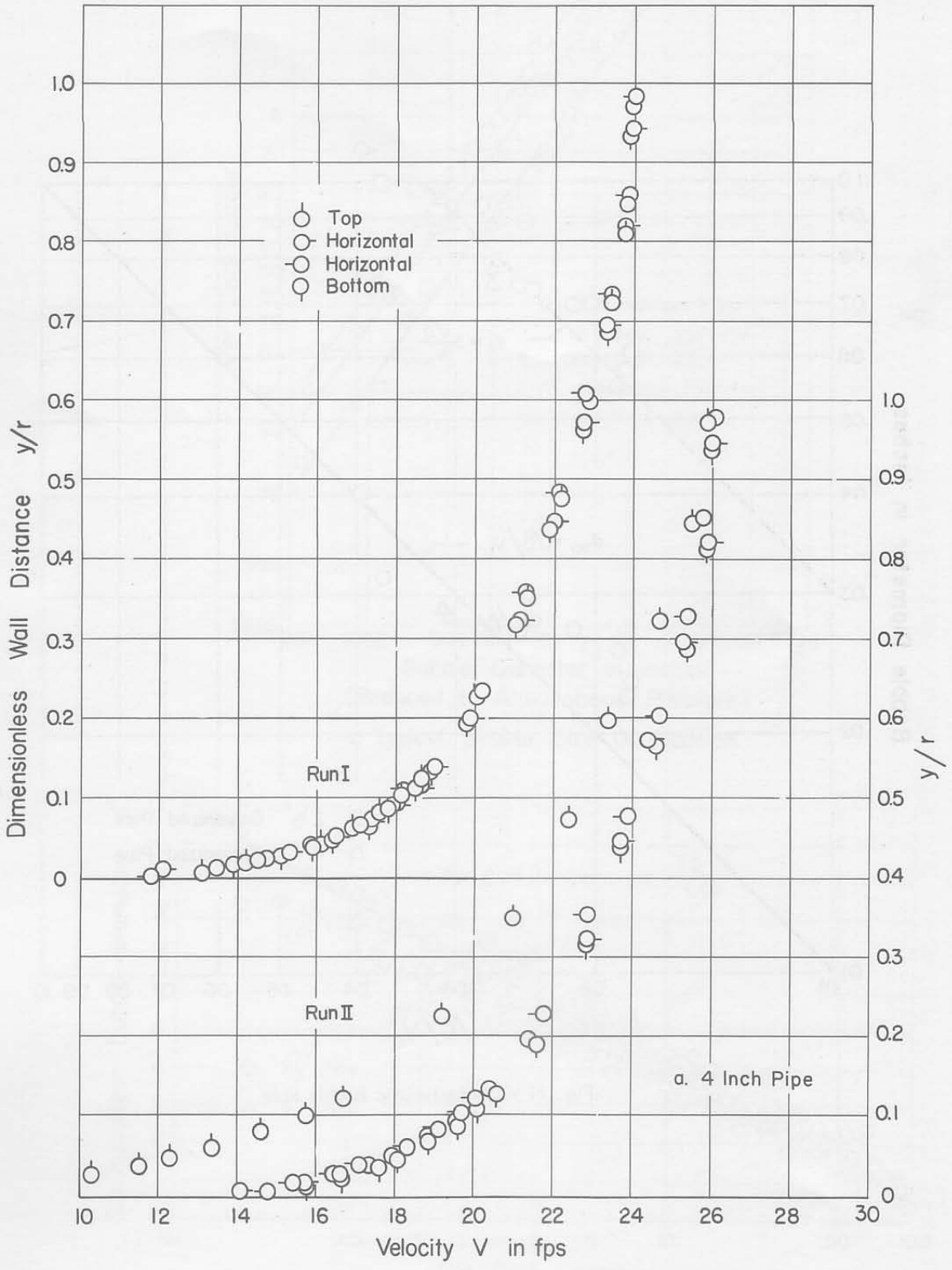

Fig. 12 - Velocity Profiles in Bubbly Mixtures

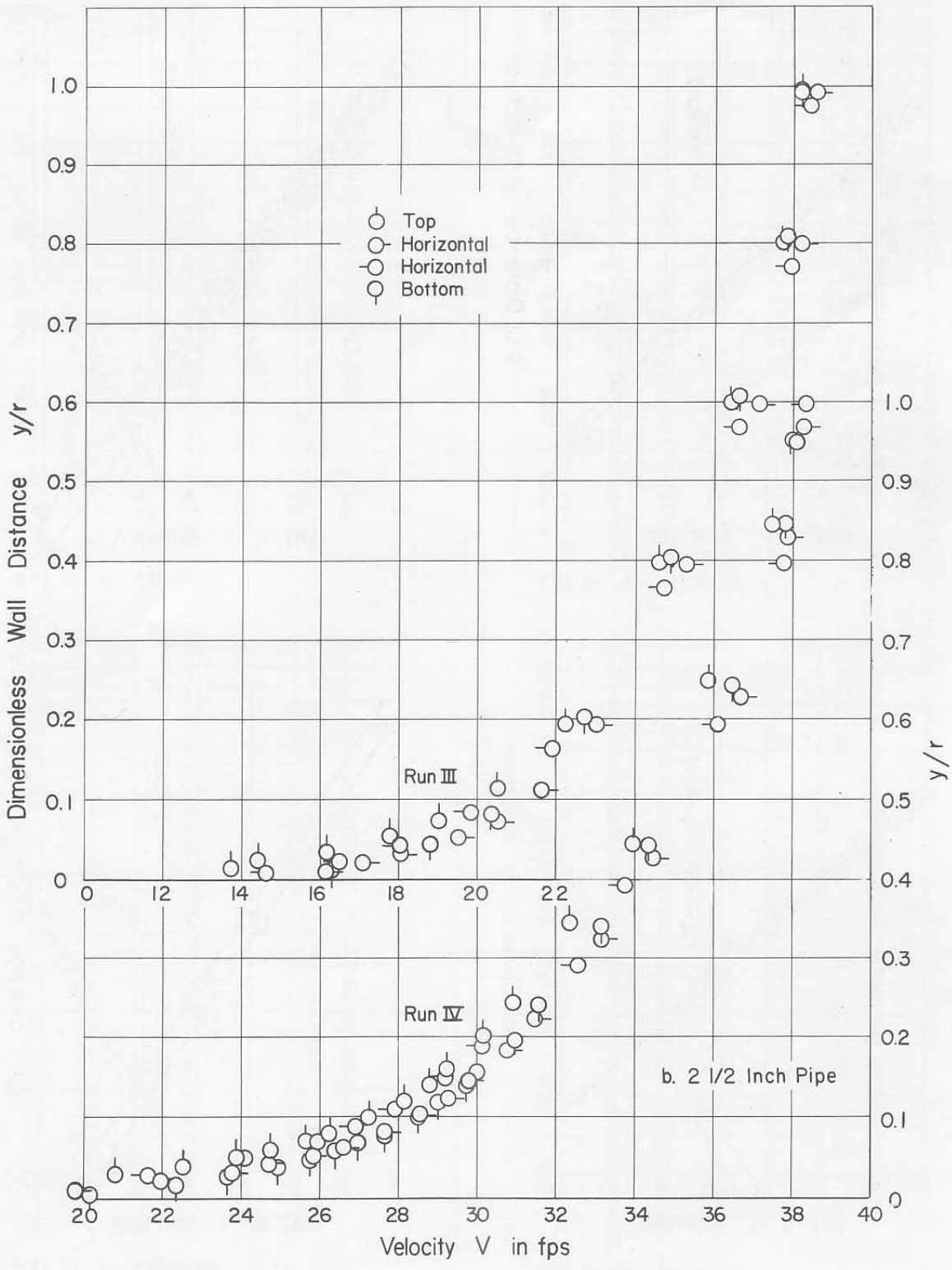

Fig. 12 (concluded) - Velocity Profiles in Bubbly Mixtures

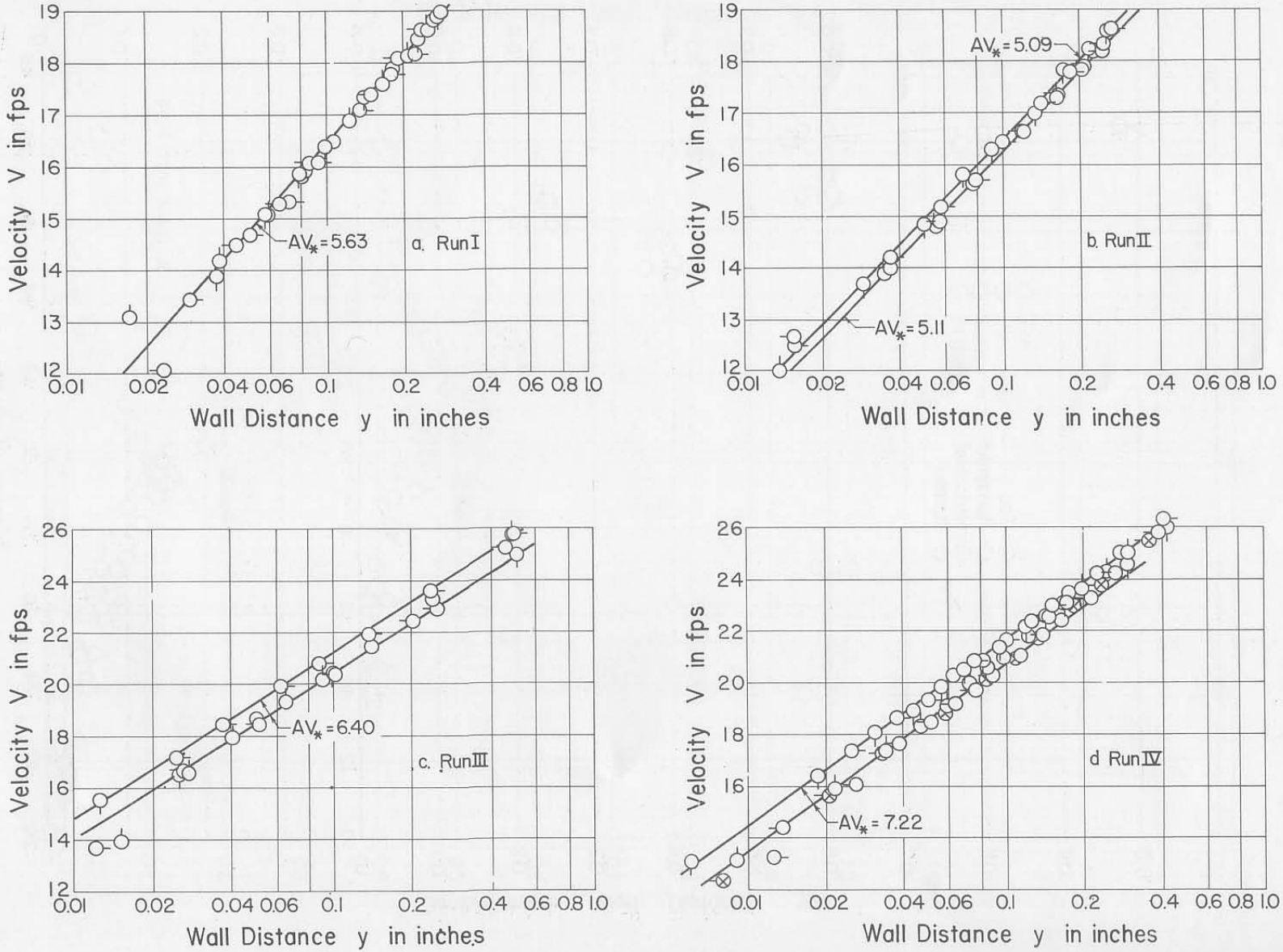

Fig. 13 - Semilogarithmic Plotting of Velocity Profiles in Pure-Water Flows

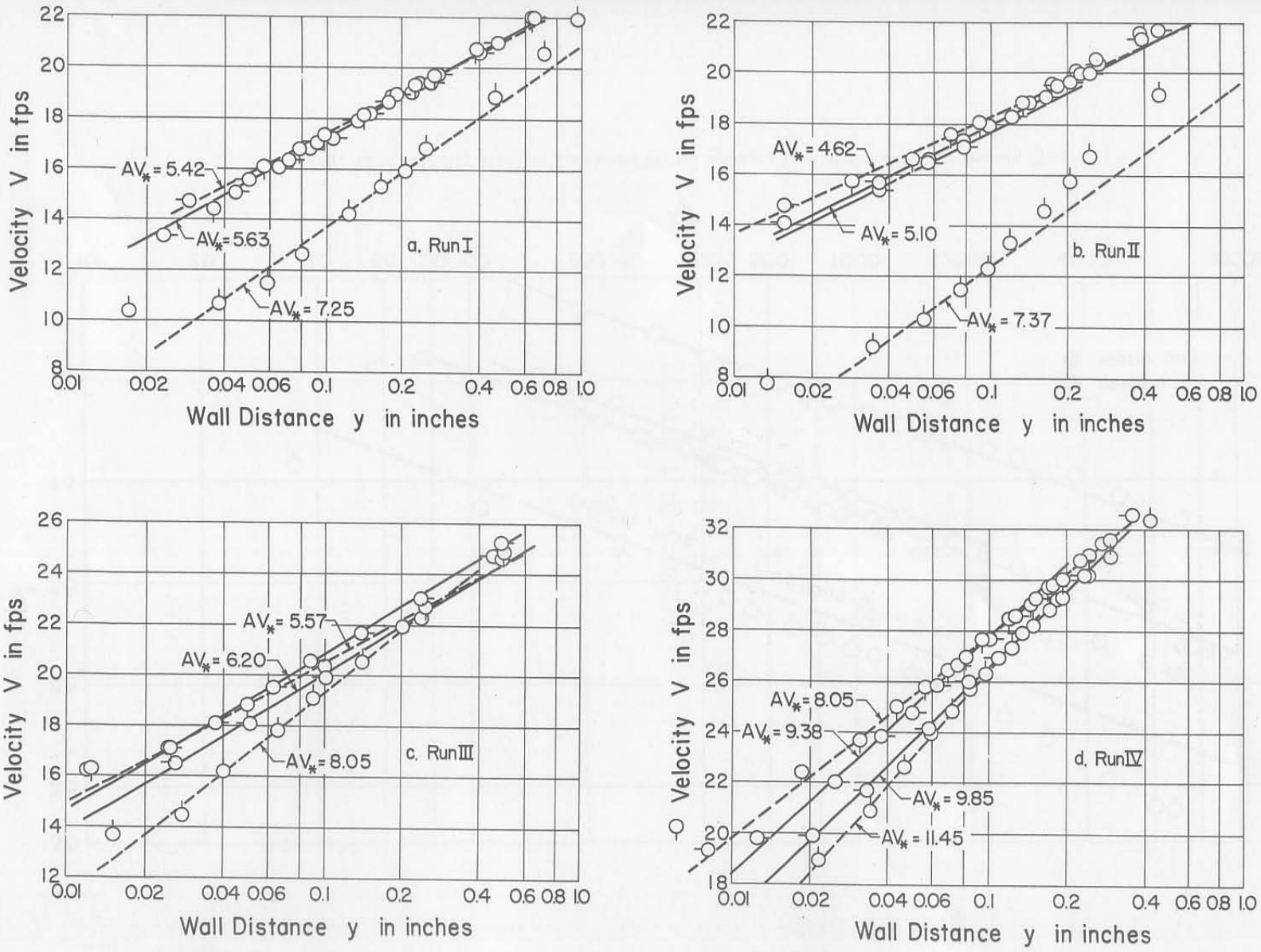

Fig. 14 - Semilogarithmic Plotting of Velocity Profiles in Air-Water Mixture Flows

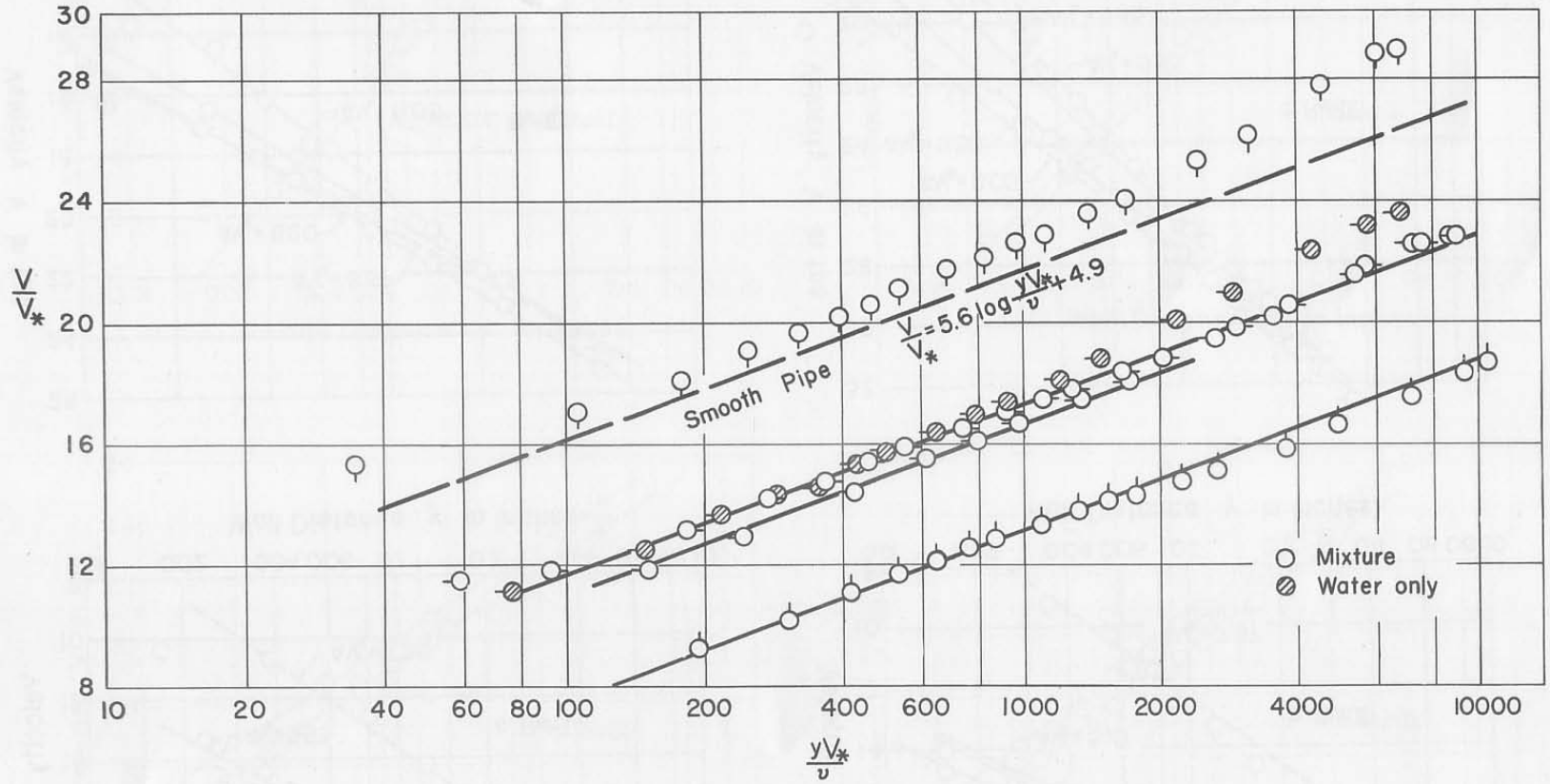

Fig. 15 - Velocity Profiles Compared With Universal Law of the Wall for Smooth Pipe

A P P E N D I X A

(Tables I through IV)

TABLE I

PRESSURE-DROP DATA AND COMPUTATIONS FOR FIRST INSTALLATION

Test No.	$T_L/T(a)$ °F	G_L/A lb/sec-ft^2	G_G/A lb/sec-ft^2	$\alpha \times 10^3$	P_o psfa	P_1 psfa	f	f/f_L	λ	θ	$1/\pi_m$
A. 2-1/2-in. Galvanized Pipe; D_i = 2.468 in., A_i = 4.784 in.^{2}, x_1 = 203.5 in.											
1*	68/68	1565	0.425	0.272	4921.9	3873.6	0.01839	1.005	1.44	0.392	0.108
2	68/68	1580	0.298	0.189	4765.0	3729.6	0.01836	1.003	1.42	0.265	0.0776
3	62/68	1530	0.461	0.302	4947.8	3916.8	0.01871	1.022	1.46	0.451	0.1177
4	62/68	1530	0.343	0.224	4716.0	3729.6	0.01844	1.008	1.43	0.335	0.0919
5	62/68	1530	0.116	0.0757	4164.5	3240.0	0.01849	1.010	1.335	0.113	0.0354
6	62/68	1555	0.299	0.192	6308.6	5342.4	0.01828	0.991	1.68	0.277	0.0569
7	62/68	1540	0.405	0.263	5672.2	4688.6	0.01822	0.996	1.58	0.386	0.0878
8	58/67	1505	0.838	0.556	5306.4	4225.0	0.01852	1.012	1.52	0.851	0.201
9	58/67	1475	1.000	0.678	5469.1	4369.0	0.01889	1.032	1.54	1.076	0.237
10	58/67	1475	0.820	0.556	5205.6	4153.0	0.01864	1.019	1.505	0.883	0.204
11	58/67	1475	0.626	0.425	4929.1	3937.0	0.01831	1.001	1.465	0.675	0.165
12	66/68	765	0.275	0.360	2711.5	2390.4	0.01880	1.027	1.10	2.07	0.247
13	66/68	825	0.218	0.265	2488.3	2145.6	0.01857	1.014	1.05	1.316	0.200
14	66/68	1320	0.494	0.374	4428.0	3600.0	0.01871	1.021	1.38	0.734	0.163
15	62/68	700	0.150	0.214	2440.8	2203.2	0.01916	1.047	1.06	1.457	0.160
16	62/68	743	0.0915	0.1232	2437.9	2188.8	0.01910	1.043	1.06	0.750	0.0923
17	62/68	1280	0.199	0.1555	5535.4	4875.8	0.01798	0.982	1.58	0.323	0.0516
18	62/68	1330	0.233	0.175	5601.6	4881.6	0.01813	0.991	1.59	0.337	0.0579
19	33/83	1170	0.804	0.687	3236.2	2430.7	0.0186	1.039	1.20	1.658	0.397
20	33/83	1170	0.725	0.620	3187.2	2406.5	0.0186	1.040	1.19	1.497	0.363
21	33/83	1170	0.625	0.535	3134.1	2386.8	0.0187	1.042	1.185	1.291	0.317
22	33/83	1170	0.515	0.440	3052.4	2351.6	0.0184	1.030	1.17	1.062	0.267
23	33/83	1170	0.445	0.381	2999.9	2324.1	0.0184	1.027	1.17	0.919	0.234
24	33/83	1170	0.370	0.316	2942.7	2295.7	0.0183	1.023	1.155	0.762	0.198
25	33/83	1170	0.256	0.219	2916.2	2324.2	0.0180	1.003	1.155	0.529	0.137
26	33/83	1170	0.180	0.154	2775.9	2197.6	0.0183	1.020	1.12	0.372	0.1015
27	33/83	1170	0	0.000	2535.5	2035.2	0.0179	1.000	--	0.000	0.0000
28	33/84	1130	0.516	0.457	3447.5	2828.0	0.01816	1.025	1.26	1.179	0.239
29	33/84	1130	0.451	0.400	3402.6	2797.5	0.01824	1.030	1.26	1.030	0.211
30	33/84	1130	0.370	0.327	3321.6	2748.5	0.01791	1.011	1.245	0.842	0.176
31	33/84	1130	0.267	0.236	3237.1	2698.2	0.01769	0.999	1.23	0.609	0.1305
32	33/84	1130	0.184	0.163	3182.7	2663.3	0.01781	1.006	1.22	0.421	0.0915
33	33/84	1130	0.120	0.106	2990.7	2485.7	0.01787	1.009	1.18	0.272	0.0632
34	33/84	1130	0	0.000	2832.0	2368.3	0.01771	1.000	--	0.000	0.0000
35	33/84	1350	0.941	0.698	3635.0	2580.6	0.01832	1.046	1.26	1.259	0.368
36	33/84	1350	0.845	0.626	3569.6	2555.9	0.01823	1.041	1.25	1.130	0.335
37	33/84	1350	0.760	0.563	3518.6	2537.5	0.01822	1.041	1.24	1.016	0.304
38	33/84	1350	0.671	0.498	3462.7	2513.8	0.01824	1.042	1.23	0.899	0.273
39	33/84	1350	0.564	0.417	3387.2	2483.4	0.01816	1.037	1.22	0.753	0.233
40	33/84	1350	0.445	0.330	3296.6	2445.2	0.01800	1.028	1.21	0.595	0.188
41	33/84	1350	0.357	0.265	3227.1	2409.2	0.01800	1.028	1.20	0.478	0.154
42	33/84	1350	0.252	0.187	3086.9	2316.1	0.01780	1.017	1.175	0.338	0.113
43	33/84	1350	0.171	0.127	2934.4	2193.7	0.01779	1.016	1.12	0.229	0.0809
44	33/84	1350	0	0.000	2734.2	2079.9	0.01751	1.000	--	0.000	0.0000
45	33/82	1510	1.063	0.705	4109.2	2793.0	0.01861	1.057	1.325	1.015	0.335
46	33/82	1510	0.980	0.650	4048.6	2765.8	0.01857	1.055	1.32	0.936	0.313
47	33/82	1510	0.915	0.606	3988.6	2734.6	0.01850	1.051	1.31	0.872	0.295
48	33/82	1510	0.850	0.564	3945.7	2715.3	0.01851	1.051	1.295	0.813	0.277
49	33/82	1510	0.765	0.507	3872.2	2681.0	0.01841	1.045	1.29	0.730	0.254
50	33/82	1510	0.676	0.448	3788.4	2636.4	0.01831	1.040	1.28	0.646	0.229
51	33/82	1510	0.575	0.381	3713.5	2604.1	0.01830	1.039	1.27	0.549	0.1975
52	33/82	1510	0.444	0.294	3577.3	2526.1	0.01819	1.033	1.245	0.423	0.1587
53	33/82	1510	0.356	0.236	3447.2	2439.2	0.01800	1.022	1.225	0.340	0.132
54	33/82	1510	0.260	0.172	3294.0	2337.0	0.01779	1.010	1.20	0.248	0.100
55	33/82	1510	0.178	0.118	3198.7	2277.0	0.01781	1.011	1.18	0.170	0.0706
56	33/82	1510	0.1245	0.0825	3133.3	2241.0	0.01773	1.007	1.17	0.119	0.0503
57	33/82	1510	0.0765	0.0507	3069.3	2215.0	0.01743	0.990	1.16	0.073	0.0314
58	33/82	1510	0	0.0000	3005.3	2180.4	0.01761	1.000	--	0.000	0.0000
59	33/83	1515	0.772	0.510	4560.3	3464.7	0.01808	1.037	1.43	0.731	0.208
60	33/83	1515	0.723	0.477	4516.0	3436.8	0.01804	1.035	1.42	0.684	0.1965
61	33/83	1515	0.671	0.444	4482.0	3413.2	0.01811	1.039	1.42	0.637	0.184
62	33/83	1515	0.626	0.414	4441.8	3391.4	0.01802	1.034	1.41	0.594	0.173
63	33/83	1515	0.570	0.376	4373.0	3339.6	0.01800	1.033	1.40	0.538	0.160
64	33/83	1515	0.510	0.337	4314.5	3299.4	0.01798	1.032	1.39	0.483	0.145
65	33/83	1515	0.436	0.288	4223.2	3239.6	0.01780	1.021	1.38	0.413	0.126
66	33/83	1515	0.370	0.244	4132.0	3162.8	0.01790	1.027	1.36	0.349	0.109
67	33/83	1515	0.260	0.172	3958.4	3033.7	0.01768	1.014	1.35	0.247	0.0805
68	33/83	1515	0.185	0.122	3869.9	2968.1	0.01773	1.017	1.32	0.175	0.0584
69	33/83	1515	0.117	0.0774	3771.1	2900.8	0.01757	1.008	1.30	0.111	0.0380
70	33/83	1515	0	0.0000	3632.9	2812.3	0.01743	1.000	--	0.000	0.0000
71	33/82	1510	0.514	0.340	5326.2	4373.4	0.01783	1.018	1.57	0.492	0.115
72	33/82	1510	0.449	0.297	5254.2	4310.5	0.01792	1.023	1.56	0.429	0.1013
73	33/82	1510	0.372	0.246	5157.6	4229.7	0.01794	1.024	1.545	0.356	0.0858
74	33/82	1510	0.270	0.179	4998.3	4097.2	0.01786	1.019	1.52	0.260	0.0646
75	33/82	1510	0.195	0.129	4868.9	3994.0	0.01769	1.010	1.50	0.186	0.0476
76	33/82	1510	0.1265	0.0839	4742.3	3889.0	0.01759	1.004	1.48	0.121	0.0319
77	33/82	1510	0	0.0000	4532.6	3715.9	0.01752	1.000	--	0.000	0.0000
B. 4-in. Galvanized Pipe, D = 4.026 in., A_i = 12.73 in.^{2}, x_1 = 87.00 in. Average f_L = 0.01428											
78	33/67	1230	0.421	0.343	3800	3659.5	0.0145	1.016	1.38	0.740	0.150
79	33/67	1240	0.361	0.291	3720	3582.1	0.0143	1.002	1.365	0.619	0.130
80	33/67	1230	0.279	0.227	3557	3423.1	0.0145	1.016	1.33	0.491	0.1064
81	33/67	1235	0.252	0.204	3514	3383.4	0.0141	0.988	1.33	0.437	0.0966
82	33/67	1240	0.224	0.181	3479	3349.7	0.0141	0.988	1.32	0.385	0.0867
83	33/67	1250	0.177	0.142	3404	3275.2	0.0141	0.988	1.30	0.298	0.0695
84	33/67	1265	0.128	0.101	3343	3213.7	0.0141	0.988	1.29	0.206	0.0503
85	33/67	1285	0.050	0.039	3255	3125.7	0.0141	0.988	1.27	0.077	0.0200
86	33/67	1310	0	0.000	3268	3136.0	0.0142	0.995	--	0.000	0.0000
87	33/70	1235	0.419	0.339	3788	3645.5	0.0146	1.023	1.375	0.726	0.149
88	33/70	1160	0.270	0.233	3388	3267.0	0.0145	1.016	1.30	0.563	0.1145
89	33/70	1170	0.216	0.185	3303	3183.5	0.0145	1.016	1.285	0.441	0.0931
90	33/70	1190	0.168	0.141	3247	3127.5	0.0143	1.002	1.27	0.326	0.0724
91	33/70	1210	0.088	0.0727	3152	3032.5	0.0144	1.009	1.255	0.162	0.0385
92	33/70	1320	0	0.000	3252	3119.4	0.0141	0.988	--	0.000	0.0000
93	33/70	1090	0.426	0.391	3037	2933.7	0.0148	1.037	1.23	0.391	0.0777
94	33/70	1130	0	0.000	2884	2782.7	0.0146	1.023	--	0.000	0.0000
95	33/70	1230	0.900	0.731	3778	3638.7	0.0144	1.009	1.375	0.731	0.149
96	33/70	1230	0.665	0.540	3617	3480.3	0.0146	1.023	1.345	0.540	0.1156
97	33/70	1230	0.545	0.442	3499	3367.7	0.0144	1.009	1.32	0.442	0.0975
98	33/70	1230	0.469	0.380	3430	3302.0	0.0142	0.995	1.31	0.380	0.0856
99	33/70	1230	0.356	0.289	3339	3213.6	0.0142	0.995	1.29	0.289	0.0668
100	33/70	1230	0.209	0.170	3220	3097.3	0.0143	1.002	1.27	0.170	0.0410
101	33/70	1230	0.0628	0.051	3101	2981.4	0.0144	1.009	1.245	0.051	0.0127
102	33/70	1230	0	0.000	3073	2957.3	0.0142	0.995	--	0.000	0.0000

*Runs 1 through 18 are a miscellaneous collection of runs that include high back pressures and forced as well as aspirated air. Average f_L = 0.0183.

TABLE II

PRESSURE-DROP DATA AND COMPUTATIONS FOR SECOND INSTALLATION

2-1/2-in. Galvanized Pipe; D_i = 2.468 in., A_i = 4.784 in.^{2}, X_{1-A} = 12.01 ft, X_{1-B} = 12.00 ft
Test Length "B" Upstream

Test No.	Section	G_0/A lb/sec-ft^2	$\alpha \times 10^3$	P_o psfa	P_1 psfa	f	f/f_L	λ	θ	$1/\pi_m$	Top	Middle	Bottom
G_L/A = 342 lb/sec-ft^2, T_L = 534.7° R													
141	A	0	0	2399	2369	0.01725	1.000		0	0			
	B	0	0	2817	2786	0.01844	1.000		0	0			
142	A	0.333	0.974	2376	2314	0.02052	1.190	1.050	29.62	0.7369	S	I	C
	B	0.344	1.006	2857	2857	0.000043	0.023	1.158	30.58	0.6246	S	I	C
143	A	0.664	1.94	2378	2295	0.01899	1.101	1.047	58.97	1.473	S	B	C
	B	0.676	1.98	2803	2785	0.00459	0.249	1.144	60.13	1.257	S	I	C
144	A	1.053	3.08	2411	2314	0.01622	0.940	1.051	93.41	2.312	S	B	C
	B	1.022	2.99	2897	2861	0.00721	0.391	1.16	90.67	1.841	S	I	C
145	A	1.300	3.80	2374	2259	0.01603	0.929	1.041	115.1	2.907	S	B	C
	B	1.302	3.80	2817	2774	0.00708	0.384	1.14	115.3	2.412	S	I	C
146	A	1.665	4.86	2397	2259	0.1563	0.906	1.043	147.3	3.704	S	B	C'
	B	1.730	5.05	2802	2754	0.00622	0.337	1.14	153.3	3.232	S	I	C
147	A	2.160	6.31	2387	2210	0.0165	0.956	1.038	190.9	4.872	S	I	B
	B	2.160	6.31	2820	2749	0.00873	0.474	1.14	190.9	4.022	S	B	C
G_L/A = 484 lb/sec-ft^2, T_L = 534.7° R													
148	A	0	0	2671	2614	0.01683	1.000		0	0			
	B	0	0	3339	3278	0.01784	1.000		0	0			
149	A	0.319	0.660	2649	2559	0.01783	1.059	1.10	10.04	0.4495	S	B	C
	B	0.336	0.695	3390	3317	0.01552	0.870	1.253	10.55	0.3670	S	B	C
150	A	0.761	1.577	2653	2515	0.01844	1.096	1.097	23.98	1.084	S	B	C
	B	0.736	1.522	3420	3389	0.00505	0.283	1.241	24.05	0.8039	S	B	C
151	A	1.034	2.14	2656	2492	0.01816	1.079	1.099	32.48	1.474	S	B	C'
	B	1.041	2.15	3380	3328	0.00694	0.389	1.244	33.98	1.154	S	B	C
152	A	1.393	2.88	2657	2468	0.01729	1.027	1.088	46.09	2.029	S	I	B
	B	1.400	2.89	3396	3313	0.00907	0.508	1.250	43.91	1.530	S	B	C'
153	A	1.905	3.94	2673	2419	0.01740	1.034	1.093	59.62	2.741	S	I	B
	B	1.890	3.91	3394	3256	0.01222	0.685	1.249	59.32	2.088	S	I	B
154	A	2.310	4.78	2642	2323	0.01772	1.053	1.080	72.28	3.410	S	I	B
	B	2.310	4.78	3341	3132	0.01532	0.859	1.230	72.28	2.616	S	I	B
G_L/A = 591 lb/sec-ft^2, T_L = 535.7° R													
155	A	0	0	2877	2793	0.01643	1.000		0	0			
	B	0	0	3790	3700	0.01765	1.000		0	0			
156	A	0.406	0.686	2849	2718	0.01735	1.056	1.140	6.986	0.4390	S	I	C
	B	0.384	0.649	3829	3712	0.01729	0.980	1.322	6.607	0.3065	S	I	C
157	A	0.800	1.350	2863	2680	0.01817	1.106	1.137	13.75	0.8684	S	B	C
	B	0.761	1.287	3823	3652	0.02020	1.144	1.320	13.08	0.6124	S	B	C
158	A	1.133	1.915	2888	2664	0.01814	1.104	1.139	19.45	1.227	S	B	C'
	B	1.150	1.940	3787	3605	0.01766	1.001	1.312	19.73	0.9351	S	B	C'
159	A	1.605	2.71	2886	2591	0.01848	1.125	1.130	27.52	1.762	S	B	C'
	B	1.590	2.69	3724	3521	0.01604	0.909	1.300	27.31	1.321	B'	O	B
160	A	1.875	3.17	2908	2520	0.02135	1.299	1.130	32.12	2.075	B'	O	B
	B	1.910	3.23	3783	3558	0.01590	0.901	1.308	32.77	1.566	B'	O	B
161	A	2.445	4.13	2864	2395	0.01969	1.198	1.110	41.70	2.784	B'	O	B
	B	2.445	4.13	3763	3457	0.01781	1.009	1.300	41.70	2.035	B'	O	B

Test No.	Section	G_0/A lb/sec-ft^2	$\alpha \times 10^3$	P_o psfa	P_1 psfa	f	f/f_L	λ	θ	$1/\pi_m$	Top	Middle	Bottom
G_L/A = 684 lb/sec-ft^2, T_L = 537.7° R													
162	A	0	0	3103	2994	0.01591	1.000		0	0			
	B	0	0	4152	4034	0.01740	1.000		0	0			
163	A	0.414	0.605	3078	2918	0.01683	1.058	1.182	4.621	0.3594	B'	I	C
	B	0.390	0.570	4158	4002	0.01810	1.040	1.380	4.359	0.2492	B	I	C
164	A	0.797	1.163	3086	2867	0.01791	1.126	1.178	8.891	0.6969	B'	B	C'
	B	0.788	1.150	4116	3904	0.01994	1.146	1.365	8.802	0.5122	B	O	C'
165	A	1.215	1.777	3084	2796	0.01855	1.166	1.170	13.62	1.081	B'	O	B
	B	1.197	1.750	4149	3894	0.02010	1.155	1.370	13.39	0.7772	B	B	B
166	A	1.810	2.640	3102	2791	0.01528	0.960	1.169	20.22	1.604	B'	O	B
	B	1.635	2.390	4166	3877	0.01929	1.109	1.364	18.30	1.063	B'	O	B
167	A	2.120	3.11	3110	2659	0.01910	1.200	1.160	23.76	1.925	B'	O	B
	B	2.010	2.94	4103	3776	0.01893	1.088	1.352	22.50	1.335	B'	O	B
168	A	2.520	3.68	3075	2503	0.01997	1.255	1.139	28.12	2.358	B'	O	B
	B	2.520	3.68	4131	3760	0.01836	1.055	1.353	28.12	1.667	B'	O	B
G_L/A = 1028 lb/sec-ft^2, T_L = 537.2° R													
169	A	0	0	3677	3435	0.01581	1.000		0	0			
	B	0	0	5372	5112	0.01697	1.000		0	0			
170	A	0.434	0.421	3655	3345	0.01614	1.021	1.277	1.435	0.2150	B	I	C
	B	0.430	0.420	5372	5061	0.01749	1.031	1.562	1.425	0.1433	B	I	C
171	A	0.867	0.845	3654	3261	0.01656	1.047	1.269	2.870	0.4356	B	O	C'
	B	0.861	0.840	5372	5001	0.01822	1.074	1.557	2.852	0.2886	B	B	B
172	A	1.410	1.372	3636	3127	0.01706	1.079	1.253	4.668	0.7248	B	O	C'
	B	1.258	1.227	5370	4946	0.01859	1.095	1.550	4.178	0.4252	B	B	B
173	A	1.755	1.710	3631	3026	0.01759	1.113	1.243	5.817	0.9180	B	B	B
	B	1.680	1.635	5370	4885	0.01901	1.120	1.543	5.560	0.5695	B	B	B
174	A	2.175	2.120	3647	2926	0.01779	1.125	1.239	7.197	1.151	B	B	B
	B	2.160	2.105	5370	4828	0.01880	1.108	1.540	7.161	0.7379	B	B	B
175	A	2.665	2.595	3627	2796	0.01683	1.065	1.220	8.820	1.444	B	B	B
	B	2.665	2.595	5370	4756	0.01892	1.115	1.533	8.820	0.9157	B	B	B
G_L/A = 1366 lb/sec-ft^2, T_L = 537.2° R													
176	A	0	0	3608	3201	0.01493	1.000		0	0			
	B	0	0	5655	5204	0.01659	1.000		0	0			
177	A	0.360	0.263	3618	3119	0.01453	0.973	1.256	0.5031	0.1386	B	I	C
	B	0.306	0.224	5660	5158	0.01698	1.024	1.587	0.4283	0.0738	B	O	C'
178	A	0.720	0.526	3606	3002	0.01589	1.064	1.241	1.006	0.2841	B	O	C'
	B	0.709	0.519	5660	5074	0.01783	1.075	1.580	0.9903	0.1721	B	B	B
179	A	1.107	0.810	3599	2872	0.01604	1.074	1.230	1.544	0.4453	B	B	B
	B	1.100	0.805	5660	4997	0.01828	1.102	1.580	1.534	0.2685	B	B	B
180	A	1.500	1.097	3611	2731	0.01630	1.092	1.217	2.089	0.6147	B	B	B
	B	1.452	1.062	5660	4930	0.01852	1.116	1.571	2.022	0.3564	B	B	B

LEGEND FOR PATTERN OBSERVATIONS

B - Bubble flow.
B' - Essentially bubble flow with some slugs.
S - Slug flow.
C - Clear liquid.
C' - Clearing liquid--the very bottom of the section is clear.
I - The middle section contains a sharp or almost sharp interface.
O - The middle sections contains no definable interface.

TABLE III

CHISHOLM AND LAIRD PRESSURE-DROP AND LIQUID-FRACTION DATA AND COMPUTATIONS

Test No.	G_0/A lb/sec-ft^2	$\alpha \times 10^3$	P/x_1 lb/ft^3	P_m psfa	σ_F^T	f	f/f_L	λ	θ	$1/\pi_m$	R_L	V_0/V_L
A. Smooth Tube; D_i = 1.062 in.; x_1 = 8 ft												
G_L/A = 39 lb/sec-ft^2; f_L = { 0.0382 for runs 1-4; 0.0372 for others												
1	0.121	3.10	0.31	2289.6	62	0.0216	0.565	1.05	7063	2.35	0.656	4.48
2	0.210	5.19	0.47	2275.2	62	0.0214	0.561	1.045	12,230	4.10	0.339	2.10
3	0.391	10.02	0.94	2246.4	62	0.0266	0.696	1.04	20,940	7.14	0.290	2.92
4	0.536	13.77	1.25	2232.0	62	0.0246	0.644	1.035	30,960	10.67	0.267	3.88
5	1.30	33.33	1.56	2232.0	69	0.0119	0.320	1.025	74,410	26.1	0.199	6.42
6	2.16	55.5	2.96	2246.4	69	0.0147	0.395	1.03	121,100	43.2	0.172	8.96
7	3.80	97.5	5.77	2332.8	60	0.0162	0.424	1.05	204,800	73.3	0.124	10.38
8	5.36	137.5	9.20	2390.4	69	0.0180	0.484	1.06	278,700	100.6	0.107	12.06
9	6.61	169.8	12.8	2390.4	69	0.0196	0.527	1.06	334,300	124	0.078	10.50
10	9.42	241.5	19.8	2462.4	69	0.0201	0.540	1.08	448,800	172	0.064	11.78
11	13.9	356	31.7	2563.2	69	0.0201	0.540	1.10	606,200	244	0.042	10.70
12	19.2	491	43.7	2750.4	69	0.0190	0.511	1.14	761,000	314	0.030	9.84
G_L/A = 85 lb/sec-ft^2; f_L = { 0.0314 for runs 13-16; 0.0306 for others												
13	0.118	1.39	1.17	2304.0	61	0.0281	0.894	1.05	665.5	1.044	0.596	1.54
14	0.224	2.64	1.64	2275.2	61	0.0267	0.850	1.045	1262	2.00	0.468	1.76
15	0.357	4.20	2.34	2260.8	61	0.0272	0.866	1.043	2008	3.22	0.388	2.04
16	0.519	6.10	2.96	2260.8	62	0.0252	0.803	1.043	2913	4.67	0.344	2.45
17	1.28	15.05	5.00	2275.2	69	0.0189	0.618	1.035	7205	11.6	0.258	4.04
18	2.07	24.35	7.03	2304.0	69	0.0168	0.550	1.04	11,550	18.5	0.199	4.59
19	3.61	42.5	12.5	2361.6	69	0.0172	0.0562	1.057	19,790	31.6	0.175	6.70
20	5.16	60.6	17.2	2404.8	69	0.0165	0.540	1.063	27,790	44.2	0.148	7.68
21	6.68	78.5	21.5	2505.6	69	0.0161	0.526	1.088	35,380	54.9	0.124	7.77
22	9.29	109.2	29.8	2606.4	69	0.0158	0.517	1.11	47,850	73.5	0.104	8.53
23	13.9	163.5	48.4	2822.4	68	0.0170	0.556	1.153	68,250	102	0.077	8.52
24	19.7	232	66.4	3211.2	68	0.0172	0.562	1.23	91,380	130.5	0.062	8.63
G_L/A = 119 lb/sec-ft^2; f_L = { 0.0289 for runs 25-28; 0.0282 for others												
25	0.119	1.00	1.95	2318.4	62	0.0280	0.970	1.055	245.0	0.75	0.638	1.32
26	0.213	1.79	2.65	2304.0	62	0.0282	0.976	1.055	438.2	1.34	0.539	1.57
27	0.358	3.01	3.67	2289.6	62	0.0280	0.970	1.05	735.5	2.27	0.419	1.64
28	0.520	4.37	4.58	2289.6	62	0.0263	0.910	1.05	1067	3.31	0.351	1.79
29	1.23	10.33	8.12	2332.8	69	0.0226	0.801	1.047	2539	7.78	0.275	2.95
30	2.20	18.50	11.85	2376.0	69	0.0192	0.680	1.06	4505	13.6	0.234	4.16
31	3.75	31.5	17.9	2448.0	69	0.0172	0.610	1.075	7583	22.6	0.184	5.10
32	5.46	46.0	24.6	2520.0	69	0.0163	0.578	1.09	10,890	32.0	0.171	6.61
33	6.52	54.9	29.0	2592.0	69	0.0162	0.575	1.105	12,890	37.2	0.143	6.22
34	9.28	78.0	38.4	2664.0	69	0.0146	0.518	1.122	17,960	51.5	0.120	7.03
35	14.0	117.8	54.6	2937.6	69	0.0140	0.498	1.176	26,130	70.4	0.093	7.21
36	19.1	160.7	77.2	3326.4	69	0.0155	0.550	1.252	34,330	84.5	0.077	7.05
G_L/A = 185 lb/sec-ft^2; f_L = { 0.0247 for runs 49-52; 0.0242 for others												
37	0.122	0.660	3.82	2376.0	62	0.0268	1.085	1.07	66.88	0.481	0.732	1.31
38	0.206	1.113	4.84	2376.0	62	0.0278	1.125	1.07	112.9	0.812	0.614	1.29
39	0.361	1.95	6.09	2376.0	61	0.0258	1.045	1.07	197.6	1.425	0.489	1.36
40	0.526	2.87	7.80	2376.0	61	0.0260	1.052	1.07	287.7	2.01	0.445	1.61
41	1.30	7.03	12.5	2448.0	68	0.0206	0.850	1.085	715.6	5.03	0.316	2.32
42	2.18	11.80	22.3	2491.2	68	0.0198	0.818	1.095	1194	8.29	0.258	2.88
43	3.89	21.03	30.1	2592.0	68	0.0182	0.752	1.10	2112	14.2	0.234	4.34
44	5.50	29.75	42.7	2736.0	68	0.0187	0.772	1.135	2985	19.2	0.187	4.42
45	6.55	35.4	46.1	2836.8	68	0.0175	0.723	1.155	3507	21.9	0.181	4.85
46	9.45	51.1	60.0	2937.6	68	0.0155	0.640	1.175	4984	30.4	0.148	5.28
47	14.1	76.1	83.5	3398.4	68	0.0159	0.657	1.265	7263	39.2	0.122	5.45
48	19.3	104.3	99.5	3600.0	68	0.0133	0.550	1.30	9688	50.8	0.098	5.53
G_L/A = 260 lb/sec-ft^2; f_L = { 0.0237 for runs 49-52; 0.0232 for others												
49	0.122	0.470	6.40	2404.8	62	0.0251	1.060	1.075	24.10	0.338	0.784	1.23
50	0.210	0.806	7.65	2404.8	62	0.0252	1.062	1.075	41.46	0.582	0.696	1.33
51	0.359	1.38	9.60	2404.8	62	0.0250	1.055	1.075	70.84	0.993	0.584	1.39
52	0.514	1.975	11.60	2433.6	62	0.0249	1.050	1.08	101.4	1.411	0.519	1.52
53	1.30	5.00	18.6	2491.2	68	0.0206	0.888	1.085	258.3	3.52	0.379	2.14
54	2.31	8.89	26.5	2534.4	68	0.0178	0.768	1.093	457.2	6.14	0.316	2.84
55	3.87	14.9	42.9	2750.4	68	0.0188	0.810	1.14	761.5	9.48	0.262	3.36
56	5.37	20.7	57.3	2952.0	68	0.0191	0.823	1.18	1051	12.25	0.211	3.28
57	6.64	25.55	70.0	3110.4	68	0.0197	0.849	1.21	1293	14.4	0.196	3.52
58	9.60	37.0	85.8	3340.8	68	0.0171	0.737	1.255	1849	19.4	0.174	4.08
59	14.0	53.95	109.5	3758.4	68	0.0160	0.690	1.33	2653	25.1	0.144	4.225
G_L/A = 407 lb/sec-ft^2; f_L = { 0.0213 for runs 60-66; 0.0208 for others												
60	0.119	0.245	13.9	2476.8	61	0.0246	1.155	1.09	6.12	0.204	0.823	0.948
62	0.207	0.509	15.6	2505.6	61	0.0246	1.155	1.095	10.64	0.349	0.753	1.063
64	0.378	0.929	18.4	2505.6	61	0.0221	1.040	1.095	19.43	0.640	0.672	1.31
65	0.505	1.24	20.9	2505.6	61	0.0235	1.103	1.095	25.95	0.855	0.620	1.40
66	0.780	1.92	25.0	2548.8	62	0.0223	1.048	1.11	40.05	1.30	0.515	1.38
67	1.27	3.12	30.2	2649.6	69	0.0198	0.952	1.12	65.91	2.06	0.445	1.65
68	2.24	5.50	40.6	2736.0	68	0.0172	0.827	1.135	116.0	3.52	0.374	2.10
69	3.90	9.57	64.0	3196.8	68	0.0188	0.904	1.225	201.1	5.27	0.328	2.58
70	5.26	12.93	83.9	3326.4	68	0.0189	0.910	1.25	270.3	6.79	0.269	2.50
71	6.62	16.77	99.0	3456.0	68	0.0181	0.870	1.28	339.1	8.24	0.246	2.69
G_L/A = 570 lb/sec-ft^2; f_L = { 0.0195 for runs 75-81; 0.0191 for others												
75	0.122	0.214	23.2	2534.4	61	0.0220	1.125	1.10	2.28	0.146	0.866	0.944
77	0.210	0.368	27.4	2577.6	61	0.0236	1.209	1.11	3.93	0.247	0.796	0.965
79	0.368	0.645	32.0	2649.6	61	0.0239	1.223	1.13	6.89	0.421	0.714	1.051
80	0.536	0.940	33.8	2649.6	61	0.0220	1.125	1.13	10.03	0.614	0.679	1.299
81	0.780	1.37	38.1	2764.8	62	0.0213	1.090	1.155	14.59	0.855	0.591	1.234
82	1.25	2.20	47.4	3009.6	68	0.0211	1.105	1.19	23.64	1.28	0.527	1.428
83	2.21	3.88	59.3	3196.8	68	0.0185	0.968	1.23	41.72	2.12	0.421	1.543
84	3.86	6.76	86.5	3484.8	68	0.0180	0.941	1.28	72.66	3.40	0.351	1.84

TABLE III (Continued)

CHISHOLM AND LAIRD PRESSURE-DROP AND LIQUID-FRACTION DATA AND COMPUTATIONS

Test No.	G_0/A lb/sec-ft^2	$\alpha \times 10^3$	P/x_1 lb/ft^3	P_m psfa	σ_F^T	f	f/f_L	λ	θ	$1/\eta_m$	R_L	V_0/V_L
B. Galvanized Tube; D_i = 1.043 in.; x_1 = 8 ft												
G_L/A = 41 lb/sec-ft^2; f_L = 0.0376												
100	0.126	3.08	0.351	2246.4	72	0.0214	0.568	1.03	6642	2.41	0.479	2.22
101	0.217	5.30	0.624	2232.0	72	0.0246	0.654	1.025	11,070	4.18	0.358	2.34
102	0.320	7.80	1.091	2203.2	73	0.02365	0.630	1.02	16,290	6.24	0.309	2.79
103	0.545	13.30	1.327	2203.2	73	0.0236	0.626	1.02	27,860	10.63	0.297	4.49
104	0.925	22.60	1.148	2188.8	73	0.0155	0.410	1.015	46,390	18.2	0.260	6.39
105	1.37	33.40	1.87	2188.8	73	0.0133	0.352	1.015	68,000	26.9	0.243	8.63
106	2.24	54.60	3.28	2188.8	73	0.0141	0.373	1.015	108,900	44.0	0.187	10.12
107	3.80	92.70	6.86	2289.6	73	0.0180	0.480	1.04	178,400	71.4	0.135	11.13
108	5.50	134.00	11.22	2347.2	73	0.0194	0.516	1.05	248,700	100.7	0.110	12.43
109	6.83	166.5	16.2	2361.6	73	0.0220	0.584	1.055	300,300	124.5	0.097	13.39
110	9.60	234	27.8	2404.8	72	0.0256	0.681	1.065	399,000	172	0.071	13.16
111	14.6	356	43.9	2592.0	72	0.0245	0.652	1.105	552,200	243	0.0511	13.10
112	20.0	489	64.6	2808.0	71	0.0254	0.669	1.15	689,400	306	0.0378	12.05
G_L/A = 87 lb/sec-ft^2; f_L = 0.0325												
113	0.126	1.333	1.402	2289.6	72	0.0305	0.938	1.04	674.8	1.113	0.564	1.44
114	0.210	2.42	1.90	2275.2	72	0.0305	0.938	1.035	1124	1.87	0.467	1.64
115	0.374	4.30	2.96	2260.8	72	0.0313	0.963	1.03	1997	3.35	0.405	2.28
116	0.530	6.10	3.90	2260.8	72	0.0308	0.949	1.03	2825	4.75	0.365	2.73
117	0.920	10.59	5.15	2289.6	72	0.0253	0.779	1.04	4882	8.14	0.322	3.86
118	1.38	15.88	6.09	2289.6	72	0.0204	0.629	1.04	7285	12.21	0.297	5.17
119	2.19	25.2	8.89	2376.0	73	0.0196	0.604	1.06	11,460	18.7	0.202	4.73
120	3.78	43.5	15.8	2390.4	73	0.0200	0.615	1.06	19,430	32.1	0.185	7.29
121	5.05	58.0	20.9	2433.6	73	0.0196	0.604	1.07	25,600	42.1	0.159	7.95
122	6.15	70.6	26.1	2505.6	73	0.0203	0.625	1.085	30,800	49.7	0.141	8.15
123	9.65	111	40.1	2606.4	73	0.0216	0.665	1.10	46,590	75.1	0.113	9.58
124	14.1	162	59.4	2822.4	72	0.0195	0.634	1.15	65,070	101.1	0.0885	9.81
125	19.5	224	83.1	3096.0	72	0.0197	0.606	1.21	85,430	127.7	0.073	10.06
G_L/A = 123 lb/sec-ft^2; f_L = 0.0310												
126	0.124	1.009	2.415	2304.0	72	0.0313	1.010	1.04	235.1	0.772	0.660	1.50
127	0.215	1.75	2.96	2304.0	72	0.0290	0.937	1.04	407.3	1.336	0.535	1.55
128	0.372	3.02	4.36	2289.6	72	0.0299	0.965	1.04	703.8	2.33	0.430	1.76
129	0.542	4.41	5.77	2304.0	72	0.0300	0.967	1.04	1024	3.37	0.358	1.88
130	0.900	7.31	7.33	2304.0	72	0.0256	0.825	1.04	1696	5.60	0.350	3.02
131	1.42	11.54	10.45	2376.0	72	0.0247	0.796	1.06	2664	8.56	0.297	3.62
132	2.20	17.9	16.5	2390.4	72	0.0253	0.816	1.06	4102	13.18	0.251	4.42
133	3.86	31.4	25.9	2404.8	72	0.0223	0.719	1.065	7103	23.0	0.214	6.26
134	5.58	45.4	33.6	2520.0	72	0.0205	0.661	1.09	10,130	31.7	0.186	7.25
135	6.79	55.1	40.3	2577.6	72	0.0200	0.646	1.10	12,210	37.8	0.166	7.53
136	9.62	78.2	53.9	2707.2	72	0.0188	0.607	1.13	16,930	50.9	0.127	7.42
137	14.4	117	76.3	3009.6	71	0.0183	0.591	1.19	24,460	68.6	0.102	7.80
138	20.7	168	102.2	3340.8	71	0.0172	0.555	1.255	33,630	88.8	0.0895	8.73
G_L/A = 191 lb/sec-ft^2; f_L = 0.0290												
139	0.127	0.665	4.68	2376.0	72	0.0298	1.028	1.06	64.32	0.493	0.710	1.207
140	0.217	1.135	5.46	2390.4	72	0.0281	0.970	1.06	109.9	0.838	0.625	1.397
141	0.376	1.97	7.80	2390.4	72	0.0302	1.040	1.06	190.2	1.45	0.504	1.473
142	0.543	2.84	10.15	2390.4	72	0.0306	1.053	1.06	274.4	2.10	0.467	1.84
143	0.945	4.95	13.9	2390.4	72	0.0276	0.951	1.06	476.6	3.65	0.372	2.16
144	1.26	6.60	19.0	2390.4	72	0.0296	1.021	1.06	634.4	4.87	0.292	2.01
145	2.26	11.8	29.8	2505.6	72	0.0282	0.971	1.085	1132	8.32	0.261	2.94
146	3.94	20.6	43.0	2563.2	72	0.0237	0.816	1.10	1957	14.18	0.238	4.44
147	5.55	29.1	56.1	2750.4	72	0.0231	0.796	1.14	2733	18.63	0.232	5.64
148	7.00	36.6	64.6	2822.4	72	0.0211	0.726	1.155	3422	22.9	0.201	5.77
149	9.34	48.9	78.8	3009.6	72	0.0198	0.682	1.19	4513	28.7	0.153	5.18
150	14.10	73.9	106.0	3340.8	72	0.0182	0.627	1.255	6655	39.0	0.113	4.97
G_L/A = 265 lb/sec-ft^2; f_L = 0.0285												
151	0.125	0.471	7.80	2404.8	72	0.0286	1.003	1.065	23.71	0.346	0.835	1.75
152	0.210	0.794	9.52	2404.8	72	0.0296	1.038	1.065	39.82	0.581	0.697	1.34
153	0.368	1.39	12.2	2404.8	72	0.0295	1.035	1.065	69.74	1.018	0.608	1.58
154	0.520	1.96	15.3	2404.8	72	0.0304	1.068	1.065	98.49	1.44	0.540	1.69
155	0.913	3.44	22.0	2462.4	72	0.0303	1.062	1.08	172.7	2.47	0.470	2.19
156	1.36	5.14	30.1	2534.4	72	0.0309	1.085	1.09	256.8	3.57	0.365	2.05
157	2.24	8.45	42.0	2606.4	72	0.0284	0.997	1.11	421.5	5.72	0.316	2.64
158	3.91	14.8	61.4	2793.6	72	0.0259	0.908	1.15	731.2	9.30	0.251	3.12
159	5.69	21.5	80.8	2937.6	72	0.0240	0.842	1.175	1057	12.9	0.214	3.51
160	7.01	26.5	91.7	3081.6	72	0.0228	0.800	1.205	1296	15.13	0.199	3.76
161	9.56	36.1	114.2	3283.2	72	0.0210	0.736	1.24	1751	19.4	0.147	3.35
G_L/A = 417 lb/sec-ft^2; f_L = 0.0270												
162	0.126	0.302	16.7	2462.4	72	0.0273	1.011	1.075	6.14	0.216	0.857	1.294
163	0.218	0.524	19.6	2520.4	72	0.0282	1.045	1.09	10.61	0.366	0.782	1.312
164	0.369	0.885	24.0	2534.4	72	0.0291	1.079	1.09	17.96	0.615	0.705	1.47
165	0.530	1.27	27.8	2534.4	72	0.0286	1.060	1.09	25.78	0.885	0.636	1.546
166	0.900	2.16	37.4	2592.0	72	0.0288	1.066	1.10	43.75	1.47	0.540	1.725
167	1.31	3.14	49.3	2707.2	72	0.0301	1.116	1.13	63.61	2.05	0.455	1.71
168	2.24	5.38	69.5	2894.4	72	0.0292	1.082	1.17	108.5	3.28	0.375	1.97
169	3.76	9.03	97.5	3110.4	72	0.0271	1.004	1.21	181.5	5.11	0.316	2.36
170	5.33	12.79	119.7	3340.8	72	0.0251	0.930	1.255	256.4	6.74	0.278	2.60
G_L/A = 594 lb/sec-ft^2; f_L = 0.0250												
171	0.331	0.221	31.05	2606.4	71	0.0264	1.056	1.11	2.20	0.149	0.860	0.916
172	0.216	0.364	34.0	2635.2	71	0.0265	1.062	1.115	3.63	0.243	0.818	1.091
173	0.369	0.621	40.7	2678.4	71	0.0281	1.122	1.12	6.20	0.409	0.758	1.281
174	0.528	0.880	46.8	2707.2	71	0.0282	1.129	1.13	8.87	0.577	0.697	1.327
175	0.906	1.527	59.0	2822.4	71	0.0281	1.124	1.15	15.21	0.950	0.588	1.359
176	1.31	2.21	72.0	2952.0	71	0.0282	1.129	1.18	21.97	1.316	0.522	1.438
177	2.13	3.59	98.0	3182.4	71	0.0288	1.152	1.22	35.68	1.98	0.467	1.735
178	2.87	4.84	114.0	3340.8	71	0.0274	1.097	1.255	48.01	2.54	0.382	1.571

TABLE IV

BUBBLE-SIZED DATA

Runs 1M-10M, 2-1/2-in. Pipe; Runs 1A-5A, 4-in. Pipe

Bubble Dia., in. *	Per Cent Larger	d'	Bubble Dia., in.	Per Cent Larger	d'	Bubble Dia., in.	Per Cent Larger	d'	Bubble Dia., in.	Per Cent Larger	d'	Bubble Dia., in.	Per Cent Larger	d'
	1M			2M			3M			4M			5M	
$G_0/A = 0.610$, $\alpha = 0.402 \times 10^{-3}$			$G_0/A = 0.434$, $\alpha = 0.278 \times 10^{-3}$			$G_0/A = 0.305$, $\alpha = 0.192 \times 10^{-3}$			$G_0/A = 0.510$, $\alpha = 0.384$			$G_0/A = 0.178$, $\alpha = 0.128 \times 10^{-3}$		
$\lambda = 1.59$, $V_\ell = 24.3$			$\lambda = 1.55$, $V_\ell = 25.0$			$\lambda = 1.53$, $V_\ell = 25.4$			$\lambda = 1.49$, $V_\ell = 21.3$			$\lambda = 1.41$, $V_\ell = 22.3$		
0.013	88.5	1.15	0.012	78.8	1.11	0.012	84.0	1.03	0.013	82.2	0.93	0.013	83.2	1.00
0.020	66.6	1.73	0.019	61.3	1.66	0.019	65.4	1.55	0.018	67.4	1.40	0.019	71.3	1.50
0.027	55.0	2.30	0.025	48.8	2.21	0.025	52.6	2.06	0.024	58.4	1.86	0.025	59.5	2.00
0.033	31.1	2.87	0.031	29.5	2.77	0.031	29.0	2.55	0.031	40.5	2.33	0.031	37.3	2.50
0.040	15.7	3.46	0.037	19.7	3.31	0.037	20.1	3.09	0.037	28.4	2.80	0.038	26.7	3.00
0.046	7.8	4.01	0.043	14.0	3.87	0.043	14.2	3.61	0.043	19.7	3.26	0.044	18.8	3.50
0.053	4.2	4.60	0.050	9.30	4.43	0.049	10.8	4.14	0.049	13.6	3.71	0.050	14.9	3.99
0.060	2.7	5.17	0.056	6.70	4.97	0.055	7.2	4.65	0.055	9.80	4.18	0.056	10.5	4.51
0.066	1.6	5.74	0.062	5.30	5.52	0.062	5.6	5.15	0.061	7.90	4.65	0.063	8.22	5.00
0.073	1.1	6.33	0.068	3.95	6.10	0.068	4.1	5.69	0.067	6.10	5.12	0.069	6.96	5.50
0.079	0.7	6.89	0.074	2.57	6.64	0.074	2.9	6.18	0.073	4.43	5.59	0.075	4.90	6.00
0.086	0.3	7.47	0.081	1.72	7.20	0.080	1.8	6.71	0.079	3.70	6.05	0.081	3.60	6.50
0.099	0	8.61	0.087	0.86	7.76	0.086	1.1	7.22	0.085	2.40	6.52	0.088	2.84	7.00
			0.093	0.69	8.30	0.092	0.90	7.75	0.092	1.48	6.98	0.094	1.80	7.50
			0.099	0.51	8.87	0.098	0.72	8.25	0.099	1.10	7.43	0.100	1.28	8.00
			0.105	0.17	9.42	0.105	0.54	8.77	0.104	0.55	7.90	0.106	0.26	8.50
			0.112	0	9.95	0.111	0.36	9.30	0.110	0.18	8.38	0.113	0	9.00
						0.123	0.18	10.3	0.116	0	8.82			
						0.129	0	10.8						
	$d_{50} = 0.0255$			$d_{50} = 0.0224$			$d_{50} = 0.0234$			$d_{50} = 0.0272$			$d_{50} = 0.0257$	
	$s = 0.470$			$s = 0.593$			$s = 0.591$			$s = 0.576$			$s = 0.615$	
	6M			7M			8M			9M			10M	
$G_0/A = 0.230$, $\alpha = 0.203 \times 10^{-3}$			$G_0/A = 0.181$, $\alpha = 0.156 \times 10^{-3}$			$G_0/A = 0.156$, $\alpha = 0.132 \times 10^{-3}$			$G_0/A = 0.156$, $\alpha = 0.218 \times 10^{-3}$			$G_0/A = 0.095$, $\alpha = 0.125 \times 10^{-3}$		
$\lambda = 1.33$, $V_\ell = 18.2$			$\lambda = 1.32$, $V_\ell = 18.6$			$\lambda = 1.32$, $V_\ell = 19.0$			$\lambda = 1.16$, $V_\ell = 11.5$			$\lambda = 1.16$, $V_\ell = 12.2$		
0.012	89.5	0.78	0.012	88.2	0.80	0.012	90.0	0.82	0.011	97.8	0.452	0.011	94.0	0.482
0.018	73.5	1.17	0.018	75.6	1.20	0.018	75.4	1.22	0.017	93.7	0.680	0.017	72.0	0.723
0.024	63.6	1.56	0.024	64.7	1.57	0.024	61.6	1.63	0.022	89.0	0.905	0.022	66.0	0.963
0.030	45.0	1.95	0.030	50.7	1.99	0.030	48.0	2.04	0.028	69.9	1.13	0.028	60.0	1.21
0.036	32.6	2.34	0.036	42.5	2.39	0.036	34.2	2.45	0.033	56.3	1.36	0.033	48.0	1.44
0.042	24.3	2.73	0.042	34.3	2.79	0.042	27.5	2.85	0.039	46.9	1.58	0.039	40.0	1.69
0.048	18.3	3.12	0.048	26.8	3.18	0.048	21.5	3.28	0.044	40.5	1.71	0.044	32.0	1.93
0.054	11.3	3.51	0.054	20.3	3.58	0.054	13.0	3.68	0.050	38.1	2.03	0.050	26.0	2.17
0.060	9.00	3.90	0.060	16.4	3.99	0.060	9.20	4.08	0.055	33.3	2.26	0.055	20.0	2.41
0.066	8.00	4.30	0.066	13.2	4.35	0.066	7.40	4.48	0.061	29.4	2.49	0.061	20.0	2.65
0.072	6.70	4.70	0.072	9.30	4.75	0.072	4.23	4.88	0.066	27.8	2.72	0.066	18.0	2.89
0.078	5.00	5.08	0.078	7.15	5.16	0.078	3.52	5.31	0.072	23.0	2.94	0.077	16.0	3.37
0.084	3.30	5.47	0.084	5.37	5.58	0.084	2.82	5.70	0.077	19.1	3.17	0.083	10.0	3.62
0.090	2.30	5.84	0.090	3.93	5.96	0.090	2.11	6.12	0.083	14.3	3.40	0.088	6.0	3.86
0.096	1.70	6.24	0.096	3.21	6.37	0.096	1.76	6.51	0.088	13.5	3.62	0.105	4.0	4.58
0.102	1.00	6.64	0.102	2.14	6.77	0.102	1.06	6.92	0.094	11.1	3.85	0.122	2.0	5.30
0.108	0.67	7.02	0.108	1.07	7.18	0.114	0.71	7.75	0.099	8.8	4.07	0.138	0	6.02
0.120	0.33	7.80	0.114	0.72	7.58	0.120	0.35	8.15	0.105	7.9	4.29			
0.132	0	8.60	0.120	0	8.00	0.144	0	0	0.110	7.1	4.52			
									0.116	4.8	4.75			
									0.121	4.0	4.97			
									0.127	2.4	5.20			
									0.132	0.79	5.43			
									0.143	0	5.88			
	$d_{50} = 0.0268$			$d_{50} = 0.0301$			$d_{50} = 0.0279$			$d_{50} = 0.0402$			$d_{50} = 0.0320$	
	$s = 0.620$			$s = 0.654$			$s = 0.718$			$s = 0.610$			$s = 0.718$	
	1A			2A			3A			4A			5A	
$G_0/A = 0.254$, $\alpha = 0.221 \times 10^{-3}$			$G_0/A = 0.162$, $\alpha = 0.137 \times 10^{-3}$			$G_0/A = 0.304$, $\alpha = 222 \times 10^{-3}$			$G_0/A = 0.223$, $\alpha = 0.167 \times 10^{-3}$			$G_0/A = 0.100$, $\alpha = 0.075 \times 10^{-3}$		
$\lambda = 1.375$, $V_\ell = 18.5$			$\lambda = 1.36$, $V_\ell = 18.9$			$\lambda = 1.475$, $V_\ell = 21.4$			$\lambda = 1.44$, $V_\ell = 21.4$			$\lambda = 1.385$, $V_\ell = 21.4$		
0.011	89.3	0.579	0.011	84.6	0.588	0.012	89.5	0.701	0.011	85.5	0.67	0.011	91.8	0.65
0.017	75.5	0.868	0.017	74.0	0.882	0.018	72.1	1.05	0.017	74.9	1.00	0.016	78.2	0.98
0.022	67.3	1.16	0.022	64.3	1.18	0.024	61.0	1.405	0.022	64.0	1.34	0.022	69.3	1.30
0.028	54.8	1.45	0.028	50.0	1.48	0.029	45.0	1.75	0.028	49.1	1.67	0.027	52.9	1.63
0.034	44.0	1.74	0.033	41.8	1.77	0.035	33.3	2.11	0.034	38.4	2.00	0.033	45.4	1.96
0.039	37.0	2.02	0.039	31.3	2.06	0.041	25.1	2.46	0.039	29.5	2.34	0.038	32.2	2.28
0.045	29.5	2.32	0.045	26.3	2.35	0.047	21.9	2.81	0.045	24.5	2.68	0.044	22.3	2.60
0.050	23.3	2.61	0.050	20.9	2.65	0.053	16.6	3.15	0.050	18.9	3.01	0.049	14.8	2.94
0.056	17.0	2.89	0.056	17.1	2.94	0.059	14.0	3.52	0.056	16.4	3.35	0.055	10.8	3.25
0.062	13.8	3.16	0.061	13.2	3.22	0.065	10.8	3.85	0.062	13.2	3.66	0.065	9.90	3.90
0.067	12.0	3.47	0.067	11.5	3.53	0.071	7.50	4.22	0.067	10.1	4.03	0.071	9.10	4.24
0.073	10.7	3.76	0.073	8.80	3.82	0.076	4.57	4.58	0.073	7.50	4.35	0.076	6.60	4.58
0.078	8.20	4.05	0.078	6.60	4.12	0.082	4.24	4.92	0.078	6.90	4.68	0.082	4.12	4.90
0.084	7.54	4.34	0.084	4.95	4.41	0.088	2.94	5.28	0.084	5.67	5.01	0.098	3.30	5.88
0.090	6.30	4.63	0.089	4.95	4.70	0.094	2.28	5.61	0.095	4.40	5.70	0.104	1.65	6.20
0.095	5.66	4.92	0.095	3.85	5.00	0.100	1.63	5.98	0.106	3.15	6.36	0.109	0.82	6.50
0.101	5.02	5.21	0.100	2.20	5.30	0.112	1.30	6.65	0.112	2.52	6.68	0.125	0	7.50
0.106	3.15	5.50	0.106	1.65	5.59	0.118	0.65	7.01	0.123	1.89	7.35			
0.112	2.51	5.74	0.112	1.10	5.89	0.129	0.33	7.71	0.134	1.26	8.02			
0.118	1.26	6.08	0.134	0.55	7.06	0.135	0	8.08	0.140	0	8.34			
0.123	0.63	6.37	0.173	0	9.10									
0.129	0	6.65												
	$d_{50} = 0.0289$			$d_{50} = 0.0280$			$d_{50} = 0.0275$			$d_{50} = 0.0280$			$d_{50} = 0.0264$	
	$s = 0.725$			$s = 0.703$			$s = 0.610$			$s = 0.703$			$s = 0.655$	

*Corrected to atmospheric conditions using perfect gas law.

d_{50} = Geometric mean diameter, inches.

s = Logarithmic standard deviation.

APPENDIX B

LIMITING CASES OF EQUATION (17)

APPENDIX B

LIMITING CASES OF EQUATION (17)

A. Pure Liquid Flow ($G_G \rightarrow 0$)

For the gas content to approach zero implies $\alpha \rightarrow \theta \rightarrow 0$. Upon establishing the following limits

$$\lim_{G_G \rightarrow 0} \frac{\pi_o}{\pi_1} = \lim_{G_G \rightarrow 0} \frac{\pi_o + 1}{\pi_1 + 1} = \frac{P_o}{P_1}$$

$$\lim_{G_G \rightarrow 0} \theta \pi_n = \frac{gP_n}{w_L V_\ell^2}$$

it is readily shown that the limiting case of Eq. (17) as $G_L \rightarrow 0$ is

$$\frac{fx_1}{2D} = \frac{P_o - P_1}{w_L V_\ell^2} g \qquad \text{(A-1)}$$

This is the established result obtained by integrating Eq. (12).

B. Pure Gas Flow ($G_L \rightarrow 0$)

For the liquid content to approach zero implies $\alpha \rightarrow \theta \rightarrow \infty$. The following limits are required in this development

$$\left.\begin{aligned} &\lim_{G_L \rightarrow 0} \pi = 0, \qquad \lim_{G_L \rightarrow 0} \ell n \frac{\pi_o}{\pi_1} = \ell n \frac{P_o}{P_1} \\ &\lim_{G_L \rightarrow 0} \ell n \frac{\pi_o + 1}{\pi_1 + 1} = 0, \qquad \lim_{G_L \rightarrow 0} \theta \pi_n^2 = \frac{gP_n^2 A^2}{RTG_G^2} \end{aligned}\right\} \qquad \text{(A-2)}$$

$$\lim_{G_L \to 0} \theta \left(\frac{\pi_n}{1 + \pi_1} \right)^m = 0, \; m = 3, 4, \ldots$$

Equation (17) can be rewritten as:

$$\frac{fx_1}{2D} = \theta(\pi_o - \pi_1) - \ell n \frac{\pi_o}{\pi_1} - \theta \ell n \left[1 + \frac{\pi_o - \pi_1}{\pi_1 + 1} \right] + \ell n \frac{\pi_o + 1}{\pi_1 + 1} \qquad \text{(A-3)}$$

Let G_L be so small that $(\pi_o - \pi_1)/(\pi_1 + 1) < 1$. Applying the logarithmic expansion series

$$\ell n \, (1 + x) = x - \frac{x^2}{2} + \frac{x^3}{3} - \ldots, \; -1 < x \leqq 1 \qquad \text{(A-4)}$$

to $-\theta \ell n \, [1 + (\pi_o - \pi_1)/(\pi_1 + 1)]$ and combining the first two terms of this expansion with $\theta(\pi_o - \pi_1)$, Eq. (A-3) can be put in the form

$$\left. \begin{aligned} \frac{fL}{2D} = \frac{\theta(\pi_o^2 - \pi_1^2)}{2(\pi_1 + 1)^2} - \ell n \frac{\pi_o}{\pi_1} + \ell n \frac{\pi_o + 1}{\pi_1 + 1} + \\ \xi \left[\theta \left(\frac{\pi}{1 + \pi_1} \right)^n \right], \; n = 3, 4, \ldots \end{aligned} \right\} \qquad \text{(A-5)}$$

where

$$\xi \left[\theta \left(\frac{\pi}{1 + \pi_1} \right)^n \right] \to 0$$

as $G_L \rightarrow 0$. Letting $G_L \rightarrow 0$ this limiting case of Eq. (17) becomes

$$\frac{fx_1}{2D} = \frac{g(P_o^2 - P_1^2)A^2}{2RTG_G^2} - \ell n \frac{P_o}{P_1} \qquad \text{(A-6)}$$

Now $$\frac{2RTG_G^2}{gA^2} = \frac{2V_o^2 P_o w_o}{g}$$ (The subscript G has been dropped on the right)

and $$\frac{P_o}{P_1} = \frac{V_1}{V_o}$$

} (A-7)

Hence, Eq. (A-6) can be put in the form

$$P_o^2 - P_1^2 = \frac{V_o^2 P_o w_o}{g} \left[2\ell n \frac{V_1}{V_o} + \frac{fx_1}{D} \right] \qquad \text{(A-8)}$$

This is the established result for isothermal compressible flow in pipes obtained by integrating Eq. (11) using Eq. (13b).

DISTRIBUTION LIST FOR TECHNICAL PAPER NO. 26, SERIES B
of the St. Anthony Falls Hydraulic Laboratory

Copies	Organization
100	Commanding Officer and Director, David Taylor Model Basin, Washington 7, D. C., Att: Code 513.
9	Chief, Bureau of Ships, Department of the Navy, Washington 25, D. C. 5 - Technical Library (Code 312) 1 - Technical Assistant to Chief of the Bureau (Code 106) 1 - Preliminary Design (Code 420) 1 - Hull Design (Code 440) 1 - Research and Development Program Planning (Code 320)
6	Chief, Bureau of Yards and Docks, Department of the Navy, Washington 25, D. C.
2	Chief, Bureau of Aeronautics, Department of the Navy, Washington 25, D. C., Att: 1 - Aero and Hydro Branch (Code AD-3) 1 - Research Division (Code RS)
2	Chief, Bureau of Ordnance, Department of the Navy, Washington 25, D. C., Att: 1 - Assistant for Aero, Hydro, and Ballistics (Code Re03) 1 - Underwater Missile Branch (Code ReU1)
3	Chief of Naval Research, Department of the Navy, Washington 25, D. C., Att: Mechanics Branch (Code 438).
1	Director, U. S. Naval Research Laboratory, Washington 25, D. C., Att: Code 2021.
1	Commanding Officer, Office of Naval Research, Branch Office, The John Crerar Library Building, 10th Floor, 86 East Randolph Street, Chicago 1, Illinois.
1	Commander, U. S. Naval Ordnance Laboratory, White Oak, Silver Spring, Maryland.
1	Commander, U. S. Naval Ordnance Test Station, 3202 East Foothill Boulevard, Pasadena, California.
1	Commanding Officer and Director, U. S. Navy Underwater Sound Laboratory, Fort Trumbull, New London, Connecticut.
1	Superintendent, U. S. Naval Postgraduate School, Monterey, California, Att: Librarian.
1	Chief of Research and Development, Department of the Army, Washington 25, D. C.

Copies	Organization
1	Director, U. S. Waterways Experiment Station, P. O. Box 631, Vicksburg, Mississippi.
1	Office of the Chief of Engineers, Department of the Army, Gravelly Point, Washington 25, D. C.
5	Director, National Aeronautics and Space Administration, 1512 H Street, N. W., Washington 25, D. C.
1	Director, Langley Research Center, NASA, Langley Field, Virginia.
1	Director, Lewis Research Center, NASA, 21000 Brookpark Road, Cleveland 35, Ohio.
1	Director, Hydraulic Laboratory, Bureau of Reclamation, Denver Federal Center, Denver, Colorado.
5	Commander, Armed Services Technical Information Agency, Arlington Hall Station, Arlington 12, Virginia, Att: TIPDR.
2	Director, National Bureau of Standards, National Hydraulic Laboratory, Washington 25, D. C.
2	Newport News Shipbuilding and Dry Dock Company, Newport News, Virginia. For distribution as follows: 1 - Assistant Naval Architect 1 - Director, Hydraulics Laboratory
1	Chief, Engineering Research Division, Colorado State University, Fort Collins, Colorado.
1	California Institute of Technology, Division of Engineering, Pasadena 4, California, Att: Dr. M. S. Plesset, Professor of Applied Mechanics.
2	Dr. John Breslin, Davidson Laboratory, Stevens Institute of Technology, 711 Hudson Street, Hoboken, New Jersey.
1	Professor L. J. Hooper, Director, Alden Hydraulic Laboratory, Worcester Polytechnic Institute, Worcester 2, Massachusetts.
1	Dr. A. T. Ippen, Director, Hydrodynamics Laboratory, Massachusetts Institute of Technology, Cambridge 39, Massachusetts.
1	Professor Laurens Troost, Head, Department of Naval Architecture and Marine Engineering, Massachusetts Institute of Technology, Cambridge 39, Massachusetts.
1	Director, Woods Hole Oceanographic Institute, Woods Hole, Massachusetts, Att: Dr. C. O. Iselin, Senior Oceanographer.
1	Dean M. P. O'Brien, Department of Engineering, University of California, Berkeley 4, California.

Copies	Organization
1	Dr. Hunter Rouse, Director, Iowa Institute of Hydraulic Research, State University of Iowa, Iowa City, Iowa.
1	S. Logan Kerr and Company, 1520 Bethlehem Pike, Flourton, Pennsylvania, Att: Mr. S. Logan Kerr.
1	Allis Chalmers Company, Milwaukee, Wisconsin, Att: Mr. Wm. J. Rheingans.
1	Director, Engineering Societies Library, 29 West 39th Street, New York 18, New York.
2	Library, California Institute of Technology, Pasadena, California.
1	Librarian, Massachusetts Institute of Technology, Cambridge 39, Massachusetts.
2	Librarian, Library of Congress, Washington 25, D. C.
1	Librarian, School of Engineering, University of Texas, Austin, Texas.
2	Director, Ordnance Research Laboratory, Pennsylvania State University, University Park, Pennsylvania.
3	Serials Division, University of Minnesota Library, Minneapolis, Minnesota.
1	Dr. W. D. Baines, Head, Hydraulic Laboratory, National Research Council, Ottawa, Ontario, Canada.
1	Director, Netherlands Ship Model Basin, Haagsteeg 2, Wageningen, The Netherlands.
1	Director of Research, British Shipbuilding Research Association, 5 Chesterfield Gardens, Curzon Street, London, W1, England.
1	Dr. H. W. Lerbs, Director, Hamburg Model Basin, Branfelder Str. 164, Hamburg 33, Germany.
1	Dr. Hans Edstrand, Director, Statens Skeppsprovningsanstalt, 14 Gibraltargatan, Göteborg C, Sweden.
1	Professor J. K. Lunde, Director, Skipsmodelltanken, Skipsbygging, Trondheim, Norway.
1	Mr. M. G. Hiranandani, Director, Central Water and Power Research Station, 20 Bombay Poona Road, Poona 3, India.
1	Directeur, Bassin d'Essais des Carènes, 6, Boulevard Victor, Paris XVe, France.
1	Director, Canal de Esperiencias Hidrodinamicas, Carretera de la sierra, El Pardo, Madrid, Spain.

Copies	Organization
1	Presidenza, Italian Model Basin, Via della Vasca Navale 89, Roma-Seda, Italy.
1	Chief of Cavitation Tunnel, Werkstad, Aktiebolaget Karlstads Mechaniska, Kristinehamn, Sweden.
1	Mr. Ovid Baker, Magnolia Petroleum Company, Natural Gas Department, P. O. Box 900, Dallas 21, Texas.
1	Mr. Richard Anderson, Reactor Engineering Division, Argonne National Laboratory, Box 299, Lemont, Illinois.
1	Professor A. D. K. Laird, University of California, Berkeley, California.
1	Dr. D. Chisholm, 4 Mount Road, Cosby, Leicester, England.